Beyond Trotterization: Variational Product Formulas for Quantum Simulation

Ibsal Assi, Michael Vogl, 2,3 Meenu Kumari, 4,5,6 and J. P. F. LeBlanc^{1,7}

¹Department of Physics and Physical Oceanography, Memorial University of Newfoundland and Labrador, St. John's, Newfoundland & Labrador, Canada A1B 3X7 ²Physics Department, King Fahd University of Petroleum & Minerals, Dhahran 31261, Saudi Arabia ³Interdisciplinary Research Center (IRC) for Advanced Quantum Computing (AQC), KFUPM, Dhahran, Saudi Arabia ⁴Digital Technologies, National Research Council Canada ⁵Perimeter Institute for Theoretical Physics, Waterloo ON N2L 2Y5, Canada ⁶Institute for Quantum Computing, University of Waterloo, Ontario N2L 3G1, Canada ⁷Compute Everything Technologies Ltd., St. John's, Newfoundland & Labrador, Canada (Dated: November 20, 2025)

We propose a variational alternative to the Trotter-Suzuki decomposition that provides greater control over errors while preserving the unitary structure of time evolution. The variational parameters in our ansatz are derived from a global action principle, where Euler-Lagrange equations govern their optimal dynamics. Unlike conventional wavefunction-based variational methods, our approach specifically targets the time evolution operation and this allows a single set of optimized parameters to be applied to any initial state for a fixed Hamiltonian avoiding costly optimization procedures. Our method outperforms the standard Trotter-Suzuki formulas, typically achieving higher accuracy than higher-order Suzuki schemes. This translates directly to quantum computing applications, where it enables the design of quantum circuits with fewer gates which reduces noise and improves precision. Although we focus on quantum dynamics, the method is broadly applicable to problems involving general time-evolution operators. Applied to various model Hamiltonians, our approach reduces errors by factors of 2 to 5 compared to Trotter-Suzuki decompositions, demonstrating its promise for accurate quantum simulation with improved efficiency. In certain cases, the variational ansatz achieves higher accuracy than more complex higher-order Suzuki formulas while reducing the gate count by nearly half within a single circuit layer. Furthermore, we derive approximate analytical expressions for the variational parameters up to cubic order in time, valid for generic Hamiltonians. These approximations enable long-time quantum simulations with improved accuracy over equivalent Suzuki decompositions, providing ready-to-use evolution formulas that match Suzuki's gate complexity while delivering better performance.

I. INTRODUCTION

Many-body quantum systems are described by Hilbert spaces whose dimensions grow exponentially with system size, such as the number of particles or spins. This rapid growth severely limits the ability to simulate realistic models on classical computers. For instance, exact diagonalization of one-, two-, or three-dimensional spin systems is constrained by the exponential increase in the number of sites and spin configurations [1–3]. Quantum computers have been proposed as a promising solution to this challenge, offering the potential for significant computational advantages over classical approaches [4–6], and have therefore attracted considerable interest [7–10]. A key task in this context is the accurate simulation of quantum time evolution under a given time-independent Hamiltonian H, as this is essential for understanding the dynamical and static properties of quantum systems.

In digital quantum simulation (DQS), the time evolution operator of H, $U(t) = e^{-iHt}$, is implemented by decomposing it into a sequence of discrete unitary operations, or quantum gates. Typi-

cally, this operator cannot be expressed directly in terms of the elementary gates available on a quantum computer. The Trotter-Suzuki (TS) decomposition addresses this challenge by systematically approximating U(t) as a product of simpler unitaries, each of which can be mapped into a sequence of gate operations in the corresponding quantum circuit. In the case of long time evolutions, one ideally chooses a valid trotterization for a small time step then repeat the same unitary multiple times until the full time interval is covered. This approximation introduces a controllable error that can be reduced by decreasing the time step, providing a flexible and systematic framework for digital quantum simulation [11, 12].

However, the practical utility of TS methods on near-term quantum devices is severely limited by the large quantum circuit depths required for accurate long-time evolution. Indeed, accuracy depends on local error bounds per time step; obtaining highly accurate results requires taking many small time steps, which yields deep quantum circuits (QCs). Often, this results in projected computation times that exceed the coherence times of the current Noisy Intermediate-Scale Quantum (NISQ)

processors [13, 14]. This problem necessitates the use of alternative (variational) methods that permit the design of shallower QCs.

A significant body of work has explored variational principles applied directly to a given quantum state. Methods like the Variational Quantum Eigensolver (VQE) [15–18], adapted for dynamics, and the McLachlan's variational principle minimize the error between the time derivative of a parameterized wavefunction ansatz $|\psi(\boldsymbol{\theta}(t))\rangle$ and the exact Schrödinger evolution $-iH|\psi(\boldsymbol{\theta}(t))\rangle$ [19]. These methods have shown promise for simulating specific types of evolution, particularly for states slowly varying in a constrained manifold.

Nonetheless. wavefunction-based variational methods possess inherent limitations. Their accuracy is often state-dependent, optimized for a particular initial state rather than an entire unitary U(t) and the full Hilbert space. This issue renders them unsuitable for applications requiring knowledge of the full time-evolution operator, such as simulating the dynamics of arbitrary states. Moreover, it complicates the implementation in quantum gates, or in algorithmic error suppression techniques like probabilistic error cancellation, where an exact unitary structure is crucial. Furthermore, they can be susceptible to local minima and optimization challenges inherent in variational quantum algorithms [20, 21].

In this work, we overcome some of these limitations by introducing a global variational principle that applies directly to the unitary time-evolution operator itself [22]. Our approach optimizes a parameterized unitary $U(\boldsymbol{c}(t))$ to best satisfy the operator Schrödinger equation over an entire time interval. This yields a set of differential equations for the variational parameters $\boldsymbol{c}(t)$, given physically motivated initial conditions. This shift in perspective—from local, state-based error to global, operator-based error—represents a fundamental departure from both Trotter-Suzuki and wavefunction variational methods, leading to substantial improvements in accuracy and efficiency, as we shall demonstrate.

This paper is structured as follows. We begin by introducing the theoretical framework of our method and the different forms of the parametrized time-evolution ansatz. We then demonstrate its application on three representative systems: a two-level toy model for pedagogical clarity, the quantum Ising model (QIM) as a paradigmatic case in quantum simulation, and the non-integrable XXZ model with next-nearest-neighbor interactions to highlight the robustness of our method. Subsequently, we illustrate the construction of the quantum circuit for our variational ansatz using the QIM as a concrete example. Next, we discuss approximate variational tech-

niques that reduce computational costs, including the derivation of analytical expressions for the variational parameters which offer improved accuracy over Trotter–Suzuki formulas. We conclude with a summary of our results and an outlook on future research directions.

II. METHODOLOGY

In this section, we describe how to derive the equations of motion for the variational parameters of a general time-evolution ansatz using an action principle. We then introduce several parameterized product formulas for the time-evolution operator, where each unitary factor can be implemented as a sequence of elementary quantum gates. Finally, we discuss how long-time simulations can be carried out using stroboscopic time steps, making our approach directly applicable to quantum circuit implementations.

A. Quantum dynamics from action principles

The exact time evolution operator U(t) for a given Hamiltonian H, which we assume as time-independent throughout this work, fulfills the Schrodinger equation (SE),

$$i\partial_t U = HU. \tag{1}$$

We have adopted the unit system where $\hbar = 1$ throughout this work. One way to derive this equation is via the action [22]

$$S = \int dt \mathcal{L}_1 = \int dt \operatorname{Tr} \left[U^{\dagger} (i\partial_t U - HU) \right]. \tag{2}$$

The Schrödinger equation can be derived by minimizing the action with respect to the entries of $U^{\dagger}(t)$. As with any valid variational principle, this framework can be used to reduce computational complexity by restricting the dynamics to a carefully chosen ansatz, $U_a(t)$. In practice, $U_a(t)$ is parametrized using a small set of variational parameters—far fewer than the total number of independent entries in the full unitary matrix U(t). Such a parametrization not only provides a computationally efficient representation of the time-evolution operator but can also offer additional physical insight into the system's dynamics. This approach is particularly relevant for quantum computing, where the goal is to implement Uon a quantum device using standard quantum gate operations. For example, in digital quantum simulations (DQS), one typically chooses an ansatz that both approximates the exact time-evolution operator and is naturally suited for implementation on a quantum circuit, as is the case with the well-known Trotter-Suzuki decomposition [23, 24]. Inspired by this structure, we adopt a similar strategy and express our ansatz for the time-evolution operator as a product of exponentials, as will be discussed in more detail in Section IIB. Crucially, our ansatz is parameterized by a set of time-dependent variational parameters, $\{c_j(t)\}$. By minimizing the action S with respect to these parameters, we obtain the corresponding equations of motion that govern their dynamics [22]

$$\sum_{k} g_{jk}\dot{c}_k + iF_j = 0 \tag{3}$$

where $g_{jk} = \text{Tr}\left[\left(\frac{\partial U_a}{\partial c_j}\right)^\dagger \frac{\partial U_a}{\partial c_k}\right]$ is the quantum geometric tensor (or mass matrix), which encodes the overlap between tangent vectors in the parameter space of the ansatz and determines the geometry of its evolution [22, 25, 26], and $F_j = \text{Tr}\left[\left(\frac{\partial U_a}{\partial c_j}\right)^\dagger H U_a\right]$ is the generalized force term that represents the projection of the Hamiltonian's action onto the variational manifold, driving the time evolution of the parameters. The solutions to these equations can be obtained using standard numerical techniques, such as Runge-Kutta integration. In certain cases, it is even possible to derive exact or approximate analytical solutions for the variational parameters, as we will demonstrate in later sections.

It is important to note that the action introduced above is not unique. In fact, there exist infinitely many possible action principles that yield the exact dynamics and can serve as starting points for a given parameterized time-evolution ansatz. A few such alternatives are listed in Appendix B. Throughout this work, we primarily focus on the action principle (\mathcal{L}_1) introduced above.

In the next section, we will discuss various forms of variational ansatz for the time-evolution operator that have direct applications to quantum computing.

B. Time-evolution ansatz

In this section, we explore a special class of unitary ansatz that can be easily translated into a quantum circuit. As a first scenario, we assume that our Hamiltonian H is decomposed into two noncommuting terms A and B. Here, ideally A or B consist of a linear combination of terms that are mutually commuting. The goal is to approximate the time-evolution operator as a product of unitary operators made from A and B where each unitary can be implemented as a set of gate operations in a quantum of the second of the

tum circuit. For such an ansatz the only computational errors would be due to neglecting the nonzero commutator [A, B]. We consider the following variational ansatz for the time-evolution operator:

$$U_a(t) = \prod_{j=0}^{\mathcal{M}} e^{ic_{2j}(t)A} e^{ic_{2j+1}(t)B},$$
 (4)

where \mathcal{M} is an integer that controls the circuit depth and can be tuned to balance expressiveness and computational cost. The coefficients $\{c_k(t)\}$ are real-valued variational parameters, which ensures that $U_a(t)$ remains unitary which is essential for quantum computing applications. We should note Trotter-Suzuki decomposition is a special case of this ansatz for which $c_{2j}(t) = c_{2j+1}(t) = -t/(\mathcal{M}+1)$ and taking $\mathcal{M} \to \infty$, $U_a(t)$ recovers the full (exact) time-evolution.

For finite-dimensional quantum systems such as spin models, there exists a fundamental mathematical guarantee that for sufficiently large but finite \mathcal{M} , this product ((4)) can exactly equal U(t) for all times t. This follows from Lie-algebraic considerations: the operators iA and iB generate a finite-dimensional matrix algebra (a closed algebraic structure under commutation), and the time evolution operator U(t) traces a continuous path within the corresponding matrix Lie group (the set of all possible unitary evolutions generated by this algebra). Since the generated Lie group forms a smooth, finite-dimensional manifold, and our product formula provides a parameterization with $2\mathcal{M} + 1$ free parameters, once \mathcal{M} is large enough that the number of parameters equals or exceeds the dimension of this manifold, exact representation becomes possible [27, 28]. For finite-dimensional spin systems, the required \mathcal{M} is bounded by the dimension of the Lie algebra generated by A and B, which is itself bounded by $\mathcal{D}^2 - 1$ where \mathcal{D} is the Hilbert space dimension [29]. This theoretical foundation ensures that variational optimization of the coefficients $c_k(t)$ can recover the exact quantum dynamics for finite \mathcal{M} .

Our variational ansatz is expected to outperform equivalent TS decompositions because it employs action principle that dynamically optimizes parameters $c_k(t)$ to satisfy the Schrödinger equation, whereas TS formulas follow fixed mathematical constructions. This physical optimization leads to enhanced accuracy for specific model Hamiltonians.

The simplest nontrivial instance of this ansatz consists of only two exponentials:

$$U_a(t) = e^{ic_0(t)A}e^{ic_1(t)B},$$
 (5)

corresponding to a single layer of alternating unitaries generated by A and B. We observe the similarity in structure to the first order Trotter-Suzuki

(TS) formula $U_{\rm TS}^{(1)}(t)=e^{-itA}e^{-itB}$. Using Eq. (3), we find the equations of motion for the variational parameters $c_{0.1}(t)$ to be

$$Tr[A^{2}](1 + \dot{c}_{0}) + Tr[AB](1 + \dot{c}_{1}) = 0$$
 (6)

$$\operatorname{Tr}[AB](1 + \dot{c}_0) + \operatorname{Tr}[B^2]\dot{c}_1 + \operatorname{Tr}[B\tilde{B}] = 0$$
 (7)

where $\tilde{B} = e^{-ic_0(t)A}Be^{ic_0(t)A}$. Note that all timeindependent traces appearing in the above equations can be evaluated analytically for arbitrary system sizes and Hamiltonian parameters, as demonstrated for the Ising and XXZ models in Appendix C. However, the dynamical trace Tr[BB] is generally nontrivial to obtain analytically and is therefore computed numerically for more general models. Accordingly, we rely on numerical solutions of the above system of differential equations. For small $c_0(t)$, one may approximate $\tilde{B} \approx B$, in which case the system admits the analytic solutions $c_0(t) = c_1(t) = -t$, corresponding to the well-known Trotter-Suzuki parameters. This serves as a useful consistency check, since in the small-t limit the variational parameters should recover the Trotter-Suzuki coefficients.

It should be noted that the performance of the ansatz in Eq. (5) depends on its operator ordering. For operators A and B, the two natural choices are the AB ordering $(U_a = e^{ic_0A}e^{ic_1B})$ and the BA ordering $(U_a = e^{ic_0B}e^{ic_1A})$. While the variational principle optimizes the parameters for either choice, one ordering typically yields a more accurate solution. The preferred choice can be determined by comparing the residual $R = ||i\dot{U}_a - HU_a||_F$, with the smaller value indicating better performance. This of course can be extended to more complicated ansatz and Hamiltonian structures.

Aside from the operator ordering, we recall the second order (symmetric) TS formula

$$U_{\rm TS}^{(2)}(t) = e^{-\frac{it}{2}A}e^{-itB}e^{-\frac{it}{2}A}.$$
 (8)

which we rely on to choose our next variational ansatz of the form

$$U_a(t) = e^{ic_0(t)A} e^{ic_1(t)B} e^{ic_2(t)A}.$$
 (9)

where we took $c_3(t) = 0$ in Eq. (4). The variational parameters $\{c_0(t), c_1(t), c_2(t)\}$ are found by solving the differential equations in Eq. (3) (or alternatively the explicit forms in Appendix A), or the ones corresponding to the other action principles discussed in Appendix B. Naturally, one can consider higher-order generalizations of this ansatz by including additional alternating exponentials, as illustrated below:

$$U_a(t) = e^{ic_0(t)A} e^{ic_1(t)B} e^{ic_2(t)A} e^{ic_3(t)B}.$$
 (10)

and so on. Increasing the number of factors allows the ansatz to capture more complex dynamics and can improve upon standard Trotterization schemes. In particular, higher-order constructions can enable accurate simulations over significantly larger time steps, as we will demonstrate later.

At first glance, adding more factors per layer appears to increase the number of quantum gates and, consequently, the circuit depth. However, the relationship is more subtle. While each layer becomes more complex, the ability to take larger time steps often reduces the total number of layers required to simulate the full evolution. Therefore, an appropriate measure is the *effective circuit depth*, which should be assessed in terms of the total gate count over the entire evolution, rather than per layer alone.

Having established this trade-off in the context of Hamiltonians that can be written as H=A+B, it is natural to ask how the method extends to systems with more intricate structures. In many physically relevant models, the Hamiltonian cannot be decomposed into only two non-commuting parts, each composed of mutually commuting operators. In such cases, it is convenient to generalize the decomposition to three or more terms.

As a concrete example, consider the XXZ Hamiltonian with both first- and second-nearest-neighbor interactions. This Hamiltonian can be partitioned into three components, A, B, and C, where A contains only the XX interaction terms, B contains only the YY interaction terms, and C contains the Ising (ZZ) terms. Each of these terms consists solely of mutually commuting operators on the N-qubit system. Consequently, the corresponding exponentials $e^{ia_j(t)A}$, $e^{ib_j(t)B}$, and $e^{ic_j(t)C}$ can be factorized exactly into parallel quantum gates, making the ansatz readily implementable on a quantum circuit.

A natural variational ansatz for this case is

$$U_a(t) = \prod_{j=1}^{M} e^{ia_j(t)A} e^{ib_j(t)B} e^{ic_j(t)C}, \qquad (11)$$

where the time-dependent variational parameters $\{a_j(t), b_j(t), c_j(t)\}$ are determined according to Eq. (3) (or using other Lagrangians as discussed in Appendix B). Such an ansatz $U_a(t)$ can be easily mapped into a sequence of quantum gate operations for quantum computing applications.

Alternatively, one can employ the ansatz in Eq. (4) in two stages. In the first stage, the Hamiltonian is partitioned into two blocks, A and B+C, leading to the ansatz

$$U_a(t) = \prod_{i=0}^{\mathcal{M}} e^{ic_{2j}(t)A}, e^{ic_{2j+1}(t)(B+C)}.$$
 (12)

In the second stage, each factor $e^{ic_{2j+1}(t)(B+C)}$ is further decomposed as an alternating product of exponentials of B and C, according to Eq. (4):

$$e^{ic_{2j+1}(t)(B+C)} = \prod_{k=0}^{\mathcal{N}} e^{id_{2k}^{(j)}(t)B}, e^{id_{2k+1}^{(j)}(t)C}.$$
 (13)

Care must be taken at this stage, since (B+C) now plays the role of an effective Hamiltonian and $-c_{2j+1}(t)$ serves as the evolution time. This distinction is essential when deriving the corresponding equations of motion. Combining the two steps, the full ansatz takes the form

$$U_a(t) = \prod_{j=0}^{\mathcal{M}} \prod_{k=0}^{\mathcal{N}} e^{ic_{2j}(t)A} e^{id_{2k}^{(j)}(t)B} e^{id_{2k+1}^{(j)}(t)C}.$$
 (14)

which is directly implementable on a quantum computer.

We will illustrate the performance of both the splitting strategies using the XXZ model in Sec. III. We will show that both the methods outperform the standard Trotter–Suzuki decomposition and yield nearly identical accuracy at short evolution times t. At longer times, however, the single-step splitting achieves lower errors. This improvement stems from its greater flexibility, as it optimizes a larger set of variational parameters simultaneously, whereas the two-step procedure effectively constrains the number of free parameters at each stage. Further numerical results and supporting analysis are presented in Sec. III.

This construction can be extended straightforwardly to Hamiltonians that decompose into more than three mutually commuting blocks. The same procedure can be readily applied to such cases.

C. Repeated evolution over multiple time periods

In digital quantum simulation (DQS), it is often necessary to simulate systems over evolution times t that exceed the time scales where a given ansatz remains accurate. Within the standard Trotter-Suzuki (TS) framework, the time-evolution operator can be approximated as

$$e^{-it(A+B)} \approx \left[e^{-i\tau A}e^{-i\tau B}\right]^n,$$
 (15)

where τ is a small time step and $n = \lfloor \frac{t}{\tau} \rfloor$. This decomposition becomes exact in the limit $\tau \to 0$ implying $n \to \infty$.

In our approach, a similar strategy can be adopted by fixing the variational parameters at $t = \tau$. For instance, using the two-parameter ansatz of Eq. (5), the evolution over a total time t can be approximated as

$$e^{-it(A+B)} \approx \left[e^{-ic_0(\tau)A}e^{-ic_1(\tau)B}\right]^n$$
. (16)

More generally, for a higher-order ansatz $U_a(\tau)$, we simply replace the product above with the full variational form,

$$e^{-it(A+B)} \approx \left[U_a(\tau) \right]^n. \tag{17}$$

This procedure enables accurate simulation of state evolution or observables over long times using a fixed, optimized ansatz at a single time step τ . As we will show in Sec. III, this approach achieves higher accuracy at larger τ compared to the conventional TS methods. Equivalently, for the same total gate count, our scheme requires fewer layers in the quantum circuit, leading to a more resource-efficient simulation.

As discussed above, there is considerable flexibility in the choice of ansatz and the ordering of operators. This flexibility allows one to select the form that yields the smallest relative error for a given problem. While it is not feasible to explore all possible configurations here, our method can be readily applied to any ansatz that may be advantageous for specific models of interest.

We summarize our algorithm in Fig. 1. In the first step, we choose a particular time evolution ansatz $U_a(c(t))$ of interest that is implementable on quantum hardware. In the second step, the variational parameters c(t) are obtained via classical optimization based on the action principle. Then, we perform error analysis to determine the optimal time (τ) for which the parameters are associated with an acceptable error bound. The output parameters $c(\tau)$ are input for quantum simulations running at stroboscopic times of size τ . This structure bears similarity to other algorithms based on McLachlan's variational principle [30]. However, our method differs in an essential way: the optimization is performed globally over the entire evolution operator rather than with respect to a specific quantum state in the Hilbert space.

The implementation of our algorithm on actual quantum hardware is beyond the scope of the present work and is left for future investigation.

III. APPLICATIONS TO VARIOUS MODELS

In this section, we demonstrate our method through three illustrative examples. We begin with a simple two-level toy model, which offers analytical insight into the core ideas of our approach. We then

Classical optimization Procedure

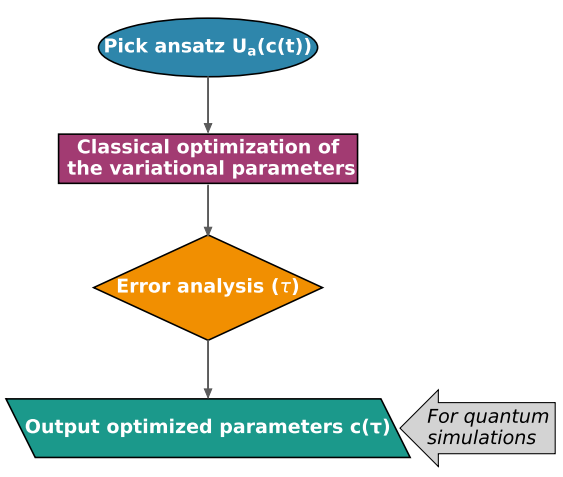


FIG. 1: Flowchart outlining the main steps of our variational algorithm. Initially, we start with a parameterize-time evolution ansatz that reflects the required complexity of the single layer in the quantum circuit. Next, the classical stage determines the variational parameters based on the action principle. Afterwards, we perform error analysis to determine the time interval where the ansatz is valid. Lastly, we generate the optimal parameters that will be then used as an input for running quantum simulations.

consider two many-body spin Hamiltonians that are generally non-integrable, except at special parameter values. For these systems, we analyze the behavior of the variational parameters and examine how the method performs as the system size increases toward the thermodynamic limit.

To quantify the accuracy of the approximate timeevolution ansatz $U_a(t)$ compared to the exact evolution U(t), we employ the following global error metric,

$$\mathcal{E}_F = \frac{1}{2\sqrt{\mathcal{D}}} \|U(t) - U_a(t)\|_F, \tag{18}$$

where \mathcal{D} denotes the Hilbert-space dimension and $||X||_F = \sqrt{\text{Tr}[XX^{\dagger}]}$ is the Frobenius norm of X. For stroboscopic dynamics, we use the analogous metric,

$$\mathcal{E}_F^{\text{Strob}} = \frac{1}{2\sqrt{\mathcal{D}}} \|U(n\tau) - [U_a(\tau)]^n\|_F.$$
 (19)

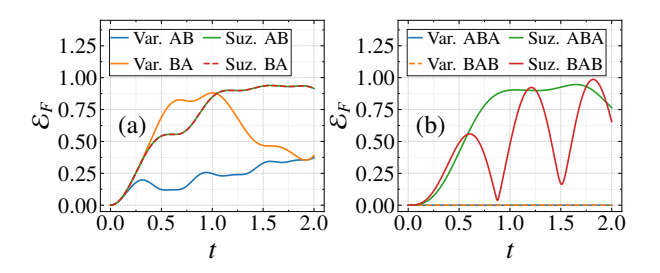


FIG. 2: (a) A plot of the normalized Frobenius norm of the difference between the exact and the approximate time-evolution, \mathcal{E}_F (Eq. (18)), for the two-level model Eq. (20) using the variational ansatz $U_a(t) = e^{ic_0A}e^{ic_1B}$ in comparison with the first order Trotter-Suzuki (TS) decomposition for both operator orderings AB and BA. (b) Similar to (a), we employ the 3-exponential variational ansatz $U_a(t) = e^{ic_0A}e^{ic_1B}e^{ic_2A}$ and compute the normalized Frobenius error against the symmetric TS formula Eq. (8) for the operator orderings ABA and BAB. Parameters: $h_x = 5$, $h_z = 2$.

A. A simple two level system

As a first example, we consider one of the simplest possible single particle Hamiltonians given by

$$H = h_x \sigma_x + h_z \sigma_z = \frac{1}{2} \vec{B} \cdot \vec{\sigma} \tag{20}$$

where $\vec{B} = (2h_x, 0, 2h_z)^T$ is a uniform magnetic field and $\vec{\sigma} = (\sigma_x, \sigma_y, \sigma_z)^T$. One can easily verify that the exact time evolution operator for this Hamiltonian is

$$U_{\text{exact}}(t) = \cos(\Omega t) - \frac{i}{\Omega}\sin(\Omega t)H \qquad (21)$$

where $\Omega = \sqrt{h_x^2 + h_z^2}$. Now, if we let $A = h_x \sigma_x$ and $B = h_z \sigma_z$, then we use the ansatz in Eqs. (5), the comparison against the equivalent first order Trotter-Suzuki (TS) formula is given in Fig. 2(a) at the different operator orderings where we simply $A \leftrightarrow B$. Meanwhile the TS results are independent of the operator orderings, we find that the variational results change with operator ordering in this case and that the case of AB ordering our variational ansatz performed best globally compared to the TS results and the variational BA ordering case. We repeated our calculations using the three-exponential ansatz in Eq. (9). As shown in Fig. 2(b), the variational approach exhibits superior accuracy compared to the symmetric Trotter-Suzuki (TS) formula of Eq. (8) with error of order 10^{-7} that originates purely from numerical inaccuracies of the Runge–Kutta integrator (RK45 in Python).

In fact, the variational approach exactly reproduces the true evolution in this case. To make this explicit, we simplify the ansatz in Eq. (9) for the present system as follows:

$$U_{\text{ansatz}}(t) = \alpha I + i\beta \sigma_x + i\gamma \sigma_y + i\lambda \sigma_z \tag{22}$$

where $\alpha = \cos(c_1h_z)\cos(h_x(c_0 + c_2))$, $\beta = \cos(c_1h_z)\sin(h_x(c_0 + c_2))$, $\gamma = \sin(c_1h_z)\sin(h_x(c_0 - c_2))$, and $\gamma = \sin(c_1h_z)\cos(h_x(c_0 - c_2))$. By setting $U_{\text{ansatz}}(t) = U_{\text{exact}}(t)$, we obtain

$$c_0(t) = c_2(t) = \frac{1}{2h_x} \tan^{-1} \left(-\frac{h_x \tan(\Omega t)}{\Omega} \right) \quad (23)$$

$$c_1(t) = \frac{1}{h_z} \sin^{-1} \left(-\frac{h_z \sin(\Omega t)}{\Omega} \right)$$
 (24)

as our unique solution. By doing Taylor expansion to linear order, we obtain $c_0(t) = c_2(t) \approx -\frac{t}{2}$ and $c_1(t) \approx -t$, these are the coefficients appearing the symmetric TS formula Eq. (8) as one would expect in the limit $t \to 0$. The above solutions cannot be obtained if one uses the simpler ansatz Eq. (5) for the fact that the equation $U_{\text{ansatz}}(t) = U_{\text{exact}}(t)$ has four equations with 2 unknowns in that case hard to satisfy all equations at once. For this system one would generally expect the need of 4 parameters in order to solve the above constraint consistently but luckily with three parameters we were able to find an analytic solution. The reasoning behind this lies in the field of Lie-Algebra following the arguments presented in the previous section. Using our variational approach (\mathcal{L}_1) , the equations of motion for our parameters are

$$q\dot{C} + b = 0 \tag{25}$$

where

$$g = \begin{bmatrix} h_x^2 & 0 & h_x^2 \cos(2c_1 h_z) \\ 0 & h_z^2 & 0 \\ h_x^2 \cos(2c_1 h_z) & 0 & h_x^2 \end{bmatrix}$$
 (26)

and

$$b = \begin{bmatrix} h_x^2 \\ h_z^2 \cos(2c_0 h_x) \\ h_x \left(h_x \cos(2c_1 h_z) + h_z \sin(2c_0 h_x) \sin(2c_1 h_z) \right) \end{bmatrix}$$
(27)

where one can easily verify that the analytic solutions in Eqs. (23) and (24) do satisfy the equations of motion Eqs. (25)-(27), indicating that the variational approach in this case recovers the analytic solutions which explains the high accuracy we obtained numerically shown in Fig. 2(b). Indeed, the alternative variational principles discussed in Appendix B yield exactly the same result. This is

expected, since all these principles are designed to reproduce the exact dynamics of the full unitary operator. In the present case of the three-exponential ansatz, the structure of the ansatz coincides with that of the exact unitary, which automatically ensures that all variational formulations produce identical parameters. Clearly, the variational approach provides more accuracy compared to using equivalent trotter-Suzuki formula. This will be clear later when using more complex models.

For many-body Hamiltonians, such analytic solutions are generally difficult to obtain, as we will see in the following sections. Nevertheless, the overall trend remains the same: increasing the number of variational parameters typically improves the accuracy of the approximation. For instance, if the Hilbert space has dimension \mathcal{D} , one would, in principle, require at least \mathcal{D}^2-1 exponentials in the alternating ansatz of Eq. (4) to fully capture the exact time evolution.

The way these parameters are assigned strongly affects the resulting quantum circuit. Increasing the number of exponentials in the ansatz can significantly enhance expressivity, but it also introduces greater gate complexity. This trade-off can, however, lead to a shallower overall circuit, since fewer Trotter steps may be needed to achieve the same simulation time. Hence, the total gate complexity considering the full circuit will be smaller. In practice, the number of exponentials in the ansatz should be chosen to balance expressivity, hardware constraints, and the dominant sources of error in the quantum device.

B. The Quantum Ising Model

Our next example is the quantum Ising model (QIM), a standard benchmark for studying quantum dynamics and digital simulation techniques [31– 33]. It is one of the simplest many-body systems that captures essential quantum effects, combining local spin interactions with non-commuting transverse and longitudinal fields. Its structure naturally matches the capabilities of modern quantum hardware, where two-qubit ZZ interactions and singlequbit rotations can be directly implemented. Moreover, in the absence of a longitudinal field $(h_z = 0)$, the model reduces to the integrable Transverse Field Ising Model (TFIM), which is analytically tractable [34]. This provides exact results for validation, while the full model with $h_z \neq 0$ still exhibits rich phenomena such as quantum phase transitions and nontrivial entanglement dynamics [35, 36]. These features make it an ideal testbed for exploring Trotterization and quantifying simulation errors. The Hamiltonian takes the form

$$H = J \sum_{j=1}^{N} S_j^z S_{j+1}^z + h_x \sum_{j=1}^{N} S_j^x + h_z \sum_{j=1}^{N} S_j^z$$
 (28)

where $S_j = \frac{1}{2} \vec{\sigma}_j$ (i.e. we are using spin 1/2 case). In this model, J controls the strength of the nearest-neighbor Ising interactions, h_x sets the magnitude of the transverse field that induces spin flips, and h_z represents a longitudinal field that breaks integrability and adds additional complexity to the dynamics. Our goal is to split the Hamiltonian into different non-commuting terms with each term consisting of mutually commuting operators. One minimal choice is by writing H = A + B, where $A = h_x \sum_{j=1}^N S_j^x$ and $B = J \sum_{j=1}^{N-1} S_j^z S_{j+1}^z + h_z \sum_{j=1}^N S_j^z$. This decomposition allows the time-evolution ansatz to be directly implemented on a quantum computer since the individual exponentials of the form $e^{ic_{2j}(t)A}$ and $e^{ic_{2j+1}(t)B}$ are easily mapped into elementary gate operations.

Figures 3(a and c) show the dynamical magnetization, $\mathcal{M}_z(t) = \frac{1}{N} \sum_j \langle \psi(t) | S_j^z | \psi(t) \rangle$, for a system initialized with all spins polarized along the z-axis, using $h_x = h_z = 1.0$ and N = 5. The results are compared between exact calculations, the symmetric second-order Trotter-Suzuki (TS) formula, and our three-exponential variational ansatz in Eq. (9). In Figs. 3(b) and 3(d), we plot the relative error in $\mathcal{M}_z(t)$ (defined as $|(\mathcal{M}_z^{\text{exact}}(t) \mathcal{M}_z^{\mathrm{method}}(t))/\mathcal{M}_z^{\mathrm{exact}}(t)|)$ obtained via the TS and the variational ansatz for both stroboscopic time steps $\tau = 0.2$ and $\tau = 0.4$, respectively. We observe that the variational approach provides a better accuracy over the TS method with a factor of 4 or 5 times better, and this advantage becomes more pronounced at larger time steps τ . While we discussed our results for the BAB operator ordering, the similar behavior was found for the ABA ordering except that the BAB ordering has the best accuracy for this model and the parameters chosen. These findings highlight the advantage of the variational approach, particularly in regimes where coarse time discretization would otherwise introduce substantial Trotter errors.

For further illustration, we compare our variational ansatz in Eq. (10) with Ruth's fourth-order formula [37, 38], given by

$$U_{\text{Ruth}}(t) = U_{\text{TS}}^{(2)}(pt) U_{\text{TS}}^{(2)}(qt) U_{\text{TS}}^{(2)}(pt),$$
 (29)

where $U_{\mathrm{TS}}^{(2)}(t)$ is the symmetric second-order Suzuki-Trotter formula in Eq. (8), with $p=\frac{1}{2-2^{1/3}}$ and q=1-2p. Figure 4(a) shows the normalized Frobenius norm results. The variational ansatz achieved lower error than the Ruth ansatz over the entire

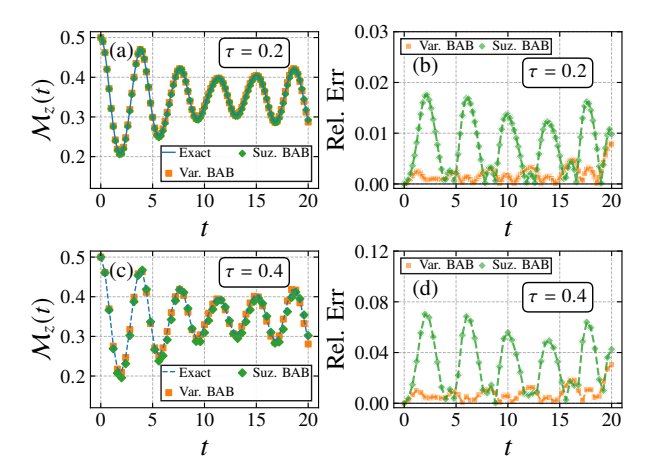


FIG. 3: (a,c) Dynamical magnetization for the QIM [Eq. (28)] comparing exact calculations, the symmetric TS formula [Eq. (8)], and our variational ansatz [Eq. (9)]. (b,d) Relative error in magnetization comparing TS and variational methods with operator ordering BAB for stroboscopic time steps of sizes $\tau = 0.2$ and $\tau = 0.4$, respectively. Parameters: $h_x = h_z = J = 1.0$, N = 5, initial state $|\psi_0\rangle = |\uparrow\rangle^{\otimes N}$.

time interval [0,2]. At t=1.0, for example, the variational ansatz yielded approximately 1.5% error, while the Ruth ansatz produced more than twice this error (over 3%). These accuracies are obtained despite the fact that we are using fewer exponentials in our variational time-evolution formula. Specifically, Eq. (29) requires seven exponentials per time step, while our variational ansatz uses only four.

To further demonstrate the practical advantage of our approach in quantum circuit implementations, we compare both ansatzes using different time steps chosen to highlight their efficiency differences. As shown in Figure 4(b), we used $\tau_{\rm var} = 0.6$ for the variational ansatz and $\tau_{\text{suz}} = 0.5$ for the Ruth ansatz, plotting the stroboscopic error over t = 40. For this simulation, the variational approach required only 68 steps compared to 81 steps for Ruth, directly translating to fewer circuit layers. More significantly, each Ruth layer contains nearly twice as many exponential operations (gates) due to its more complex structure. Consequently, the Ruth ansatz demands both more circuit layers and more gates per layer, resulting in substantially deeper quantum circuits with higher overall gate counts. To give an estimate for the gate count we assume our model has N qubits, then the exponential $e^{-i\alpha A}$ requires N R_x rotations, while $e^{-i\beta B}$ needs 2N-1 R_z rotations and 2N-2 CNOT gates. Thus, the four exponential ansatz for this particular case needs $68 \times (2N)$ R_x rotations, $68 \times (4N-2)$ R_z rotations,

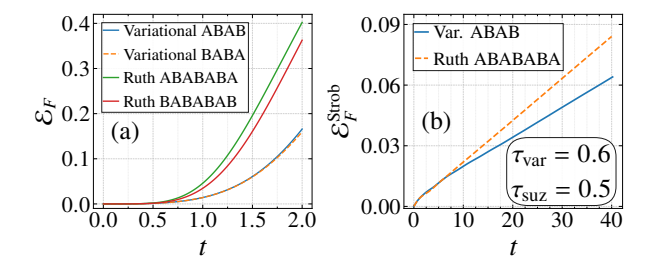


FIG. 4: (a) Normalized Frobenius norm difference between exact time evolution and approximate methods for the QIM [Eq. (28)]: variational ansatz [Eq. (10)] and Ruth's formula [Eq. (29)]. Operator orderings: variational (ABAB, BABA) and Ruth (ABABABA, BABABAB). (b) The stroboscopic error when using the variational ansatz and the Ruth decomposition with time steps of sizes $\tau_{\rm var}=0.6$, and $\tau_{\rm suz}=0.5$, respectively. Parameters: $h_x=h_z=J=1.0,\ N=5$

and $68 \times (4N-4)$ CNOT gate operations. However, for the Ruth ansatz the numbers are: $81 \times (4N)$ R_x rotations, $81 \times 3(2N-1)$ R_z rotations, and $81 \times 6(N-1)$ CNOT gate operations. This gives huge reduction in gate complexity is significant part of our variational ansatz. For example, if we consider ten-qubits QIM, using the variational ansatz in this case have $\sim 58\%$ fewer R_x gates, $\sim 44\%$ less R_z rotations, and $\sim 44\%$ reduction in CNOT operations. Our variational ansatz thus demonstrates superior performance in both accuracy and gate efficiency. We note that extending the variational framework to include more exponentials could potentially further improve accuracy and enable even larger time steps, leading to shallower circuits [39].

In addition, We calculated the the dynamical magnetization with the corresponding relative error at different time steps using the ansatz in Eq. (10) and the Ruth formula Eq. (29) with BABA and BABABAB operator orderings, respectively, as shown in Fig. 5(a,c). Clearly, we obtain better accuracy using the variational ansatz compared to the Ruth formula and this sustains at larger time steps (τ) as illustrated in the relative error in magnetization Fig. 5(b,d). This improvement is found despite the fact that we are using less exponentials in our parametrized ansatz. This further illustrates the utility of our approach for practical applications.

A natural question to ask is how the performance of the variational approach depends on the system size (i.e., the number of spins). To address this, we first considered the three-exponential ansatz in Eq. (9) and analyzed the variational parameters for the Ising model with $h_x = h_z = J = 1.0$ at $\tau = 0.5$ as shown in Fig. 6 (a,b), we plot the variational

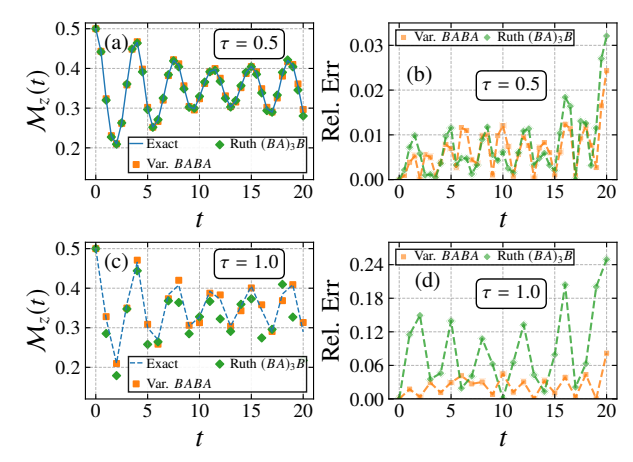


FIG. 5: (a,c) The dynamical magnetization for the QIM [Eq. (28)] obtained via exact time evolution, Ruth formula [Eq. (29)], and four exponentials variational ansatz [Eq. (10)] for different operator orderings. For the variational ansatz with ordering BABA; for Ruth with operator ordering $(BA)_3B$ (denoting BABABAB). (b,d) The corresponding relative error in the dynamical magnetization at $\tau=0.5$ and $\tau=1.0$, respectively. Parameters: $h_x=h_z=J=1.0$, and N=5, with the initial state $|\psi_0\rangle=|\uparrow\rangle^{\otimes N}$.

parameters $c_0(\tau)$, $c_1(\tau)$, and $c_2(\tau)$ as a function of 1/N for the two operator orderings ABA and BAB. Clearly, the parameters smoothly converge to well-defined values as $N \to \infty$.

We further examined the time dependence of the full set of variational parameters at different system sizes, shown in Fig. 6 (c). At short times, the parameters are largely insensitive to system size. At longer times, small deviations emerge, but the curves become increasingly closer as N grows. This indicates convergence in the thermodynamic limit to well-defined functions $c_i^{\infty}(t)$, where

$$c_j^{\infty}(t) = \lim_{N \to \infty} c_j(t). \tag{30}$$

These numerical results are consistent with the analysis in Sec. VA, where the approximate analytical formulas for the variational parameters were shown to admit a well-defined thermodynamic limit.

Having established how the variational parameters $c_j(t)$ depend on the system size N, it is also instructive to examine how the global error \mathcal{E}_F varies with N. To this end, we evaluate the normalized Frobenius error for the quantum Ising model at different system sizes and compare it with the corresponding error from the symmetric Trotter–Suzuki (TS) formula [Eq. (8)], as shown in Fig. 7. Clearly, the variational approach yields consistently lower errors across all system sizes, outperforming the equiv-

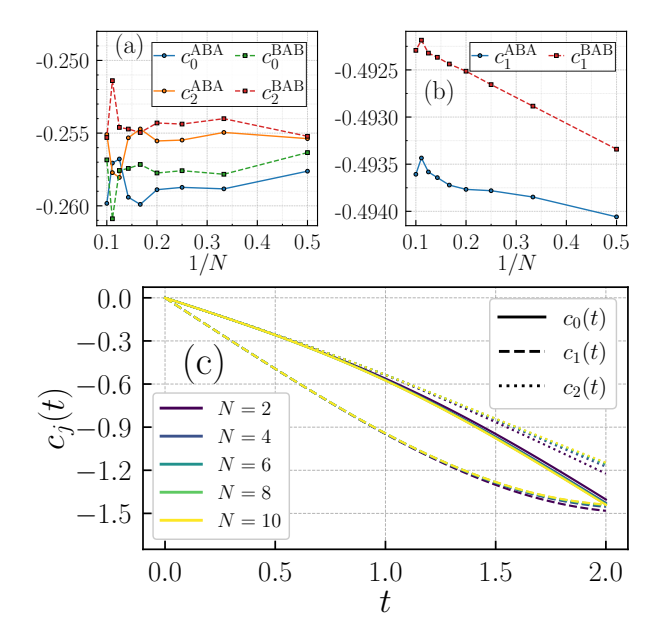


FIG. 6: (a,b) The variational parameters for the QIM [Eq. (28)] with $h_x = h_z = J = 1$ as a function of $\frac{1}{N}$ at t = 0.5 for different operator orderings. (c) A plot of the variational parameters in the ansatz Eq. (9) for the QIM [Eq. (28)] with $h_x = h_z = J = 1.0$ as a function of time t for different number of qubits, N, as indicated.

alent TS decomposition even at small t, as highlighted in the inset of the figure.

C. The XXZ model

As a final example, we consider the anisotropic Heisenberg spin chain (the XXZ model), which plays a central role in the study of strongly correlated quantum systems [40–42]. This model exhibits rich physics ranging from gapless Luttinger-liquid behavior to gapped antiferromagnetic phases, and serves as a paradigmatic setting for exploring quantum magnetism, transport, and integrability [43, 44]. In addition, extensions of the XXZ chain with next-nearest-neighbor interactions are widely used to model frustration effects in low-dimensional materials [45, 46].

The XXZ Hamiltonian is

$$H = H_{\rm NN} + H_{\rm NNN},\tag{31}$$

where the nearest-neighbor (NN) and next-nearest-

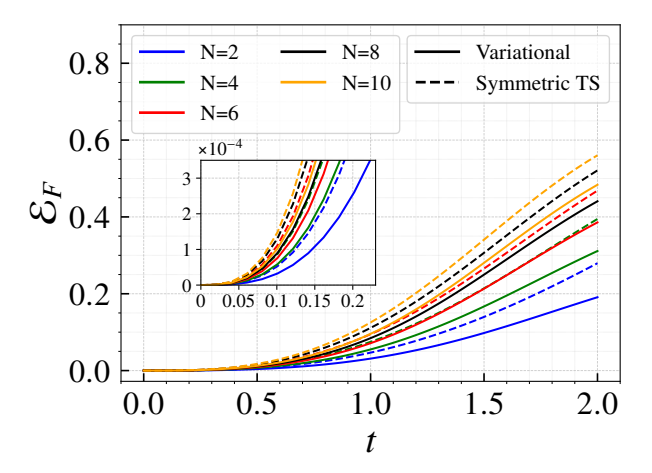


FIG. 7: Normalized Frobenius error between the exact time-evolution operator and the approximate methods for the quantum Ising model [Eq. (28)]. Results are shown for the variational ansatz [Eq. (9)] and the symmetric Trotter–Suzuki formula [Eq. (8)] using the AB operator ordering. Parameters are $J = h_z = h_x = 1$.

neighbor (NNN) contributions are given by

$$H_{\text{NN}} = J_1 \sum_{j=1}^{N-1} \left(S_j^x S_{j+1}^x + S_j^y S_{j+1}^y + \Delta_1 S_j^z S_{j+1}^z \right),$$
(32)

$$H_{\text{NNN}} = J_2 \sum_{j=1}^{N-2} \left(S_j^x S_{j+2}^x + S_j^y S_{j+2}^y + \Delta_2 S_j^z S_{j+2}^z \right).$$
(33)

Here S_j^{α} ($\alpha=x,y,z$) are spin-1/2 operators on site j. The couplings J_1 and J_2 control the strength of the nearest- and next-nearest-neighbor exchange interactions, respectively, while Δ_1 and Δ_2 parameterize the anisotropy along the z direction. For $\Delta_{1,2}=1$ the model reduces to the isotropic Heisenberg chain, and the case when $\Delta_{1,2}=0$ corresponds to the XX model.

The next step is about choosing the time-evolution ansatz for this model. At first, we focus on the simple (integrable) case without NNN interactions, $J_2 = 0$. In this case the Hamiltonian can be conveniently decomposed as a sum of two non-commuting

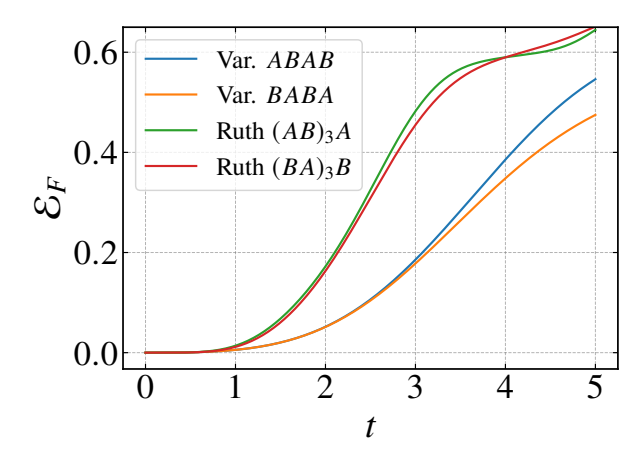


FIG. 8: Normalized Frobenius norm of the difference between exact and approximate time evolution operators for the XXZ model with only NN interaction, obtained using our four-exponential variational ansatz [Eq. (10)] and Ruth's formula [Eq. (29)] at different operator orderings. For the variational ansatz: ABAB and BABA; for Ruth: $(AB)_3A$ and $(BA)_3B$ (denoting ABABABA and BABABAB, respectively). Parameters: $J_1 = 1.0$, $\Delta_1 = 0.9$, N = 6.

terms acting on alternating bonds,

$$A = J_1 \sum_{j \text{ even}}^{N-1} \left(S_j^x S_{j+1}^x + S_j^y S_{j+1}^y + \Delta_1 S_j^z S_{j+1}^z \right),$$
(34)

$$B = J_1 \sum_{j \text{ odd}}^{N-1} \left(S_j^x S_{j+1}^x + S_j^y S_{j+1}^y + \Delta_1 S_j^z S_{j+1}^z \right).$$
(35)

This even—odd splitting is especially useful for Trotter or variational decompositions, since all terms within $A\left(B\right)$ mutually commutes with each other, allowing for efficient implementation on both classical and quantum hardware.

Figure 8 extends our analysis to the XXZ chain with parameters $J_1=1.0,\ \Delta_1=0.9,\ {\rm and}\ N=6,\ {\rm comparing}$ the Frobenius norm error of our four-exponential variational ansatz (Eq. (10)) against Ruth's seven-exponential formula (Eq. (29)). Remarkably, the variational approach maintains its superior accuracy despite requiring nearly half the number of exponentials per layer. This consistent performance across different physical models—both the quantum Ising and XXZ chains—demonstrates the robustness of our method. The observed reduction in circuit depth, coupled with enhanced precision, reinforces the variational ansatz as a versatile tool for efficient quantum simulations.

Now, we want to include the NNN interactions where we have $J_2 \neq 0$. Such a two-term splitting is no longer possible for this model. Instead, the Hamiltonian can be decomposed into into more than two parts. For example, one could choose H = A + B + C, where

$$A = J_1 \sum_{j=1}^{N-1} S_j^x S_{j+1}^x + J_2 \sum_{j=1}^{N-2} S_j^x S_{j+2}^x,$$
 (36)

$$B = J_1 \sum_{i=1}^{N-1} S_j^y S_{j+1}^y + J_2 \sum_{i=1}^{N-2} S_j^y S_{j+2}^y,$$
 (37)

$$C = J_1 \Delta_1 \sum_{j=1}^{N-1} S_j^z S_{j+1}^z + J_2 \Delta_2 \sum_{j=1}^{N-2} S_j^z S_{j+2}^z.$$
 (38)

At this stage, we proceed with one of two ways for constructing the variational ansatz either by using Eq. (11) or Eqs. ((12)-(14)). The first is a single-step split (SSS), where we use Eq. (11) and consider the ansatz,

$$U_a^{\rm SSS}(t) = e^{ic_0(t)A} e^{ic_1(t)B} e^{ic_2(t)C} e^{ic_3(t)B} e^{ic_4(t)A},$$
(39)

The second strategy is a two-step split (TSS). In the first step, we group B and C into a single block $\tilde{B} = B + C$ and employ the three-exponential ansatz of Eq. (9),

$$U_a^{\text{TSS}}(t) = e^{ic_0(t)A} e^{ic_1(t)\tilde{B}} e^{ic_2(t)A}.$$
 (40)

In the second step, the exponential $e^{ic_1(t)\tilde{B}}$ is further decomposed using another three-exponential ansatz,

$$U_1(t) = e^{ic_3(t)B} e^{ic_4(t)C} e^{ic_5(t)B}, (41)$$

where \tilde{B} plays the role of an effective Hamiltonian and $-c_1(t)$ acts as the evolution time. Together, we obtain the TSS ansatz $U_a^{\rm TSS}(t) = e^{ic_0(t)A} U_1(t) e^{ic_2(t)A}$.

To assess the performance of these approaches, we compare both ansatz with the symmetric Trotter–Suzuki formula for the XXZ model with parameters $J_1=2.0,\ J_2=0.5,\ \Delta_1=\Delta_2=0.2,$ and N=5 spins [see Fig. 9(a)]. Both variational constructions yield a clear improvement over the Trotter–Suzuki results. For this parameter set, the single- and two-step splits exhibit nearly identical accuracy, with differences becoming apparent only at larger evolution times t but this could change for other models. In general, however, the single-step split is expected to provide more robust performance across different Hamiltonian parameters as it is less constrained compared to the TSS ansatz.

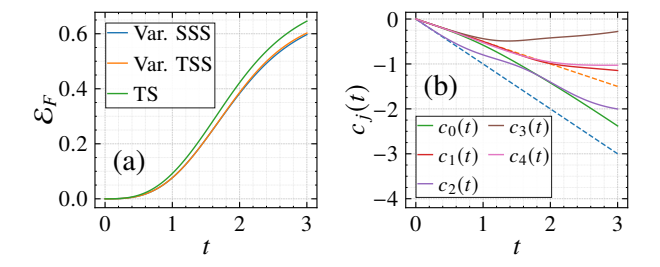


FIG. 9: (a) A comparison of the Frobenius norm errors in the time-evolution obtained with the one-step split, two-step split, and symmetric Trotter–Suzuki decompositions for the XXZ model with parameters $J_1=2.0,\,J_2=0.5,\,\Delta_1=\Delta_2=0.2,$ and N=5. (b) Variational parameters extracted from the one-step split ansatz as functions of t. The dashed blue (orange) lines correspond to the Trotter–Suzuki parameters -t (-t/2).

We have plotted the corresponding variational parameters obtained for the ansatz in Eq. (39) are shown in Fig. 9(b). At short times, the parameters follow the linear dependence prescribed by the Trotter–Suzuki formula (dashed lines). At longer times, nonlinear corrections generated by the variational procedure emerge, systematically enhancing the overall accuracy of the approximation.

To further benchmark our approach, we compare against a higher-order TS decomposition:

$$U_{\rm TS}(t) = U_{\rm BC}(t)e^{-itA}U_{\rm BC}(t), \tag{42}$$

where

$$U_{\rm BC}(t) = e^{-\frac{it}{4}C}, e^{-\frac{it}{2}B}, e^{-\frac{it}{4}C}.$$
 (43)

This TS ansatz contains seven exponentials. We construct a variational ansatz with identical structure and gate complexity:

$$U_a(t) = \prod_{i=0}^{6} e^{ic_j(t)A_j},$$
(44)

with $A_0 = A_2 = A_4 = A_6 = C$, $A_1 = A_5 = B$, and $A_3 = A$.

Figure 10(a) compares the normalized Frobenius norms, revealing that despite equivalent circuit depth, the variational approach achieves better accuracy. This advantage becomes particularly pronounced in long-time evolution, as shown in Fig. 10(b) for t=100 with $\tau=0.2$. While TS error accumulates rapidly to approximately 11% at t=100, the variational ansatz maintains substantially better accuracy ($\sim 5.5\%$)—representing a twofold improvement.

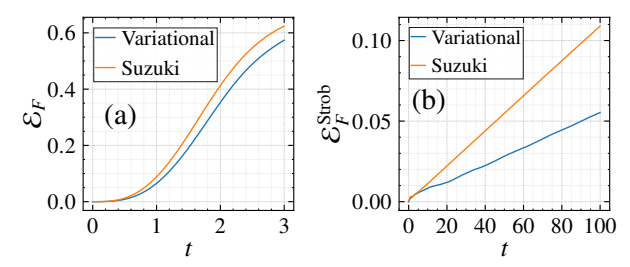


FIG. 10: (a) A comparison of the Frobenius norm errors in the time-evolution obtained using the variational scheme of Eq. (44) and the seven-exponential Trotter–Suzuki decomposition of Eq. (42) for the XXZ model with parameters $J_1 = 2.0$, $J_2 = 0.5$, $\Delta_1 = \Delta_2 = 0.2$, and N = 5. (b) Stroboscopic error growth at longer simulation times, showing that the variational approach maintains better accuracy than the TS decomposition.

Nonetheless, higher-order ansatz can be employed to improve accuracy by following the same procedure outlined above. In addition, the Hamiltonian can be partitioned into more than three blocks if needed. For example, the nearest-neighbor (NN) terms may be split into two blocks, as discussed earlier, while the next-nearest-neighbor (NNN) terms can be grouped by interaction type, with the XX, YY, and ZZ components each forming separate blocks. This yields a total of five blocks each with mutually commuting terms, for which a corresponding variational ansatz can be constructed to further enhance accuracy. Such extensions may prove useful for specific problems and are left for future investigation.

IV. BUILDING THE QUANTUM CIRCUIT FOR THE UNITARY ANSATZ

So far we have discussed the variational ansatz and its accuracy from a theoretical perspective. In practice, however, the usefulness of such an ansatz depends critically on how efficiently it can be implemented on quantum hardware. Here we demonstrate how the three-exponential ansatz in Eq. (9) can be mapped to a quantum circuit for a standard case, the quantum Ising model. For concreteness, we consider a chain of four qubits, as illustrated in Fig. 11.

The decomposition follows directly from the operator splitting introduced earlier, where we identify

$$A = h_x \sum_{j=1}^{N} S_j^x, \qquad B = J \sum_{j=1}^{N-1} S_j^z S_{j+1}^z + h_z \sum_{j=1}^{N} S_j^z.$$
(45)

The x-field contribution is implemented as single-qubit R_x rotations, while the z-field corresponds to R_z rotations. The nearest neighbor (NN) ZZ interactions are realized using a standard decomposition into a sequence of CNOT gates, a single R_z rotation, and the corresponding inverse CNOT gates between every pair of neighboring qubits. This construction makes the ansatz directly compatible with existing superconducting and trapped-ion hardware, where such two-qubit gates are natively supported.

As shown in Fig. 11, the operator operator

$$U_a(\tau) = e^{ic_0(\tau)B} e^{ic_1(\tau)A} e^{ic_2(\tau)B}$$
 (46)

is realized using layers of R_x and R_z gates interleaved with CNOT networks that generate the required NN ZZ couplings, where one can use the approximate analytic expressions of $c_j(\tau)$ given in Eq. (55) to find estimates for the elementary gate rotations. The circuit depth scales linearly with the number of qubits, and the number of variational parameters remains fixed, independent of system size. This feature highlights a key advantage of the variational ansatz: it achieves higher accuracy than a Trotter-Suzuki expansion at comparable or even reduced gate cost, while preserving an implementation that is straightforward on near-term devices.

In the next section, we introduce alternative approximate variational methods that can be implemented within our framework.

V. APPROXIMATE VARIATIONAL TECHNIQUES

This section is organized into three parts. In the first two parts, we present an approach for deriving approximate analytical expressions for the variational parameters for Hamiltonians split into two and three blocks, respectively, and show how the leading correction to the well-known Trotter–Suzuki results naturally arises. This results in alternative renormalized product formulas that can be directly used in quantum simulations for any arbitrary Hamiltonian. The third part focuses on the use of partial-trace techniques for lowering computational expenses and their connection to wavefunction-based methods.

A. Approximate Parameters for Hamiltonians Split into Two Blocks

In this section, we will discuss how to derive approximate formulas of the variational parameters for Hamiltonians of the form H=A+B. The basic idea is that we want to expand the variational

parameters in terms of Taylor series up to cubic orders to allow lowest corrections on top the the usual Trotter-Suzuki linear. Namely, we write $c_i(t) =$ $\sum_{j=1}^{3} \frac{c_{j}^{(n)}(0)}{n!} t^{n}$, where $c_{j}^{(n)}(0)$ is the nth derivative of $c_{j}(t)$ evaluated at t=0. Here we imposed the initial condition $c_i(0) = 0$ which ensures that our ansatz set to the identity at t=0. The expansion coefficients, $c_j^{(n)}(0)$, are systematically determined through successive differentiation of the equations of motion. The first-order coefficients $c_i^{(1)}(0)$ are obtained by solving Eq. (3) at t=0. Higher-order coefficients follow from temporal derivatives of the equations of motion: differentiating Eq. (3) yields $c_i^{(2)}(0)$, and a second differentiation provides $c_j^{(3)}(0)$. This approach captures essential non-linear corrections beyond the conventional Trotter-Suzuki approximation while maintaining computational tractability through the recursive structure of the derivative hierarchy. One of course can go beyond cubic corrections if necessary following exactly the same steps outlined here. For the case of our simplest ansatz in Eq. 5, the variational parameters obtained via our first action Eq. 2 are approximated to be

$$c_j(t) \approx -t + \frac{c_j^{(3)}(0)}{3!} t^3,$$
 (47)

where

$$c_0^{(3)}(0) = -2\chi \text{Tr}[AB], \quad c_1^{(3)}(0) = 2\chi \text{Tr}[A^2], \quad (48)$$

and

$$\chi = \frac{\text{Tr}[A^2 B^2] - \text{Tr}[(AB)^2]}{\text{Tr}[A^2]\text{Tr}[B^2] - (\text{Tr}[AB])^2}.$$
 (49)

with the quadratic term in the expansion fully vanishes for arbitrary model Hamiltonians. However, using other action principles, for example the one corresponding to Eq. (B1) (\mathcal{L}_2), the cubic corrections are slightly modified to be

$$c_0^{(3)}(t) \approx -2 \left[\text{Tr}[B^2] + \text{Tr}[AB] \right] \chi$$

 $c_1^{(3)}(t) \approx 2 \left[\text{Tr}[A^2] + \text{Tr}[AB] \right] \chi$ (50)

These cubic corrections are model specific and are new improvement on top the usual TS decomposition. For further analysis, we consider the three exponentials ansatz in Eq. (9), both action principles \mathcal{L}_1 and \mathcal{L}_2 gave the same results below

$$c_0(t) = c_2(t) \approx -\frac{t}{2} + \frac{c_{0,2}^{(3)}(0)}{3!} t^3,$$

$$c_1(t) \approx -t + \frac{c_1^{(3)}(0)}{3!} t^3,$$
(51)

where

$$c_0^{(3)}(0) = c_2^{(3)}(0) = -\chi \frac{\text{Tr}[B^2] + \frac{1}{2}\text{Tr}[AB]}{2},$$

$$c_1^{(3)}(0) = \chi \left[\text{Tr}[AB] + \frac{1}{2}\text{Tr}[A^2]\right].$$
(52)

The traces appearing in the above expressions can be computed analytically for the spin models at arbitrary coupling parameters and system sizes as illustrated in Appendix C. This is extremely useful for practical application to quantum computers as the variational parameters, up to a conventional factor, will decide the specific rotations of the elementary gates in the associated quantum circuit. The interested reader can easily extend these ideas to higher order ansatz and obtain approximate formulas of the associated variational parameters. In what follows, we will find the approximate variational parameters obtained via the first action principle for the spin models discussed previously.

We emphasize that these approximate formulas for the variational parameters are particularly useful in the context of Trotter-type decompositions. The unitaries $e^{ic_0(\tau)B}$ and $e^{ic_1(\tau)A}$ can be directly implemented as quantum gates, since the corresponding exponentials factorize over the qubits. In addition, the parameters $c_j(\tau)$ are available in closed analytic form as functions of the system size N and the Hamiltonian couplings, which makes them straightforward to compute for arbitrary models. This analytic accessibility ensures that the approach scales seamlessly from few-qubit setups to the thermodynamic limit, offering a practical route toward accurate large-scale simulations on future quantum devices.

1. Application to the Quantum Ising Model

In this section, we will generate the approximate variational parameters for our transverse field Ising model obtained using the \mathcal{L}_1 action principle. First, for the ansatz in Eq. (5) with BAB operator ordering, we find

$$c_0(t) \approx -t \tag{53}$$

and

$$c_1(t) \approx -t + \left[\frac{1}{12}\left(1 - \frac{1}{N}\right)J^2 + \frac{h_z^2}{6}\right]t^3$$
 (54)

where we have used the analytical traces obtained in Appendix C. Clearly, these approximate formulas have well-define thermodynamic limits which aligns

with our earlier findings in Fig. 6. The same behavior is also found when we employ our three exponentials ansatz in Eq. (9), where we find

$$c_0(t) = c_2(t) \approx -\frac{t}{2} - \frac{h_x^2}{12} \frac{J^2(N-1) + 2h_z^2 N}{J^2(N-1) + 4h_z^2 N} t^3$$

$$c_1(t) \approx -t + \frac{1}{24} \left[\left(1 - \frac{1}{N} \right) \frac{J^2}{2} + h_z^2 \right] t^3$$
(55)

The linear terms in the above formulas agree with the well-known second order (symmetric) TS formula. The cubic corrections introduced here carry more information about the given Hamiltonian and are very useful when implementing stroboscopic time-evolutions as in Eq. (17). In the language of quantum circuits, these corrections modify the elementary gate rotations for a better accuracy than the TS counterpart.

As an illustration, we benchmark the approximate variational ansatz of Eq. (55) against the symmetric Trotter–Suzuki decomposition of Eq. (8). The stroboscopic error is shown in Fig. 12. We observe that the variational construction yields a noticeably smaller error growth compared to the Trotter–Suzuki case, even for modest system sizes and time steps. This improvement highlights the advantage of tailoring the evolution operator with variational parameters, which can partially capture higher-order corrections that are absent in fixed Trotter decompositions. Further more, one can simply use the approximate variational parameters in Eq. (55) when computing any observable instead of directly employing the symmetric trotter-Suzuki formula.

2. The Integrable XXZ model

In this section, we will compute the approximate variational parameters for our XXZ model. For simplicity, we start with the integrable case where $J_2 = 0$. The relevant traces analytically in Appendix C. Using the simple two exponentials ansatz in Eq. (5), we find

$$c_0(t) \approx -t \tag{56}$$

$$c_1(t) \approx -t + \left[\frac{J_1^2}{12} \frac{1 + 2\Delta_1^2}{2 + \Delta_1^2} \frac{N - 2}{\lceil \frac{N - 1}{2} \rceil} \right] t^3$$
 (57)

while for the three exponentials ansatz (Eq. (9)), we find

$$c_{0}(t) = c_{2}(t) \approx -\frac{t}{2} - \frac{J_{1}^{2}}{48} \frac{1 + 2\Delta_{1}^{2}}{2 + \Delta_{1}^{2}} \frac{N - 2}{\left\lfloor \frac{N - 1}{2} \right\rfloor} t^{3}$$

$$c_{1}(t) \approx -t + \frac{J_{1}^{2}}{48} \frac{1 + 2\Delta_{1}^{2}}{2 + \Delta_{1}^{2}} \frac{N - 2}{\left\lceil \frac{N - 1}{2} \right\rceil} t^{3}.$$
(58)

B. Approximate Parameters for Hamiltonians Split into Three Blocks

In this section, we will discuss how to find approximate variational parameters for a general Hamiltonian $H = A + B + C = A + \tilde{B}$ based on the two step splitting discussed earlier. Basically, the first step begins with the splitting according to Eq. (40), and using the results from the previous section, we have

$$c_j(t) \approx -t + \frac{c_j^{(3)}(0)}{3!}t^3,$$
 (59)

where

$$c_0^{(3)}(0) = c_2^{(3)}(0) = -\frac{\text{Tr}[\tilde{B}^2] + \frac{1}{2}\text{Tr}[\tilde{A}\tilde{B}]}{2}\chi_1$$
 (60)

$$c_1^{(3)}(0) = \left[\text{Tr}[A\tilde{B}] + \frac{1}{2} \text{Tr}[A^2] \right] \chi_1$$
 (61)

and

$$\chi_1 = \frac{\text{Tr}[A^2 \tilde{B}^2] - \text{Tr}[(A\tilde{B})^2]}{\text{Tr}[A^2]\text{Tr}[\tilde{B}^2] - (\text{Tr}[A\tilde{B}])^2}$$
(62)

For the next step split Eq. (41), we obtain

$$c_{3,5}(t) \approx \frac{c_1(t)}{2} - \frac{c_{3,5}^{(3)}(0)}{3!}c_1^3(t)$$
 (63)

and

$$c_4(t) \approx c_1(t) - \frac{c_4^{(3)}(0)}{3!} c_1^3(t)$$
 (64)

where the cubic corrections are obtained again section VA results, giving

$$c_3^{(3)}(0) = c_5^{(3)}(0) = -\frac{\text{Tr}[C^2] + \frac{1}{2}\text{Tr}[BC]}{2}\chi_2$$
 (65)

$$c_5^{(3)}(0) = \left[\text{Tr}[BC] + \frac{1}{2} \text{Tr}[B^2] \right] \chi_2$$
 (66)

and

$$\chi_2 = \frac{\text{Tr}[B^2C^2] - \text{Tr}[(BC)^2]}{\text{Tr}[B^2]\text{Tr}[C^2] - (\text{Tr}[BC])^2}$$
(67)

These results can be easily applied to our XXZ model with NNN interactions. In fact, we have derived analytic forms of the traces appearing in these formulas for this model in Eqs. (C14)-(C23).

C. Partial traces

In quantum simulations, the physical system starts from a particular initial state $|\psi_0\rangle$ then the state evolves under the model Hamiltonian and one might be interested in looking at a dynamical observable like the magnetization in real time. Although our global approach still valid, one might get improvements by projecting out the irrelevant part of the Hilbert space using the Krylov subspace [47, 48]. For example, if we start with the actions in Eqs. (2) and (B1), and we replace the full traces with partial traces over the Krylov basis states $\{|K_j\rangle\}$, in other words, we change ${\rm Tr}\left[\cdot\right]$ to ${\rm Tr}_{\mathcal{K}}\left[\cdot\right]$, where

$$\operatorname{Tr}_{\mathcal{K}}\left[\cdot\right] = \sum_{j} \langle K_{j} | \cdot | K_{j} \rangle$$
 (68)

where the Krylov basis states are constructed from the finite vector space $\mathcal{K} = \{H^n | \psi_0 \rangle; n = 0, 1, \cdots, \mathcal{N}-1\}$, the corresponding equations of motion will be exactly similar to the previous ones except that the trace replaced with partial traces. Typically, one expects this to improve results over short period of times for smaller basis. It is also obvious that the partial traces have the advantage of being computationally less expensive than the full trace computations making it useful in certain applications.

As an illustration, we employed the idea of partial traces to compute the dynamical magnetization of the transverse-field Ising model with the ansatz in Eq. (9) and the parameters $h_x = h_z = J = 1.0$ and N=5 as shown in Fig. 13. We have considered the cases with Krylov subspace of containing one, two, and five basis vectors and we compared those results against the full variational method as shown in Fig. 13(a,c,e). Moreover, we plotted the relative error in the magnetization in Fig. 13(b,d,f). We note that using 1 Krylov state, the partial trace results where less accurate than the full variational approach over the full simulation period as clear in 13(a). However, using few more Krylov vectors, we obtained better results than the full trace method only over the first few periods as shown in 13(d,f). This is because we have constrained our variational approach to a smaller region in Hilbert space that is relevant to the initial state which we are evolving.

VI. CONCLUSIONS

In this work, we introduced a variational product formula for approximating the full time evolution of arbitrary Hamiltonians, with variational parameters determined through a globally valid variational principle [22]. Our ansatz is not only manifestly unitary but also structured as a product of elementary exponentials of local commuting terms, allowing it to be mapped directly onto standard quantum gate operations. We demonstrated that, across a range of scenarios, this approach achieves substantial improvements over standard Trotter–Suzuki decompositions. Moreover, we illustrated the flexibility of the method by applying it to systems ranging from simple models to complex many-body Hamiltonians.

We have also shown that our unitary variational ansatz can achieve higher accuracy with lower gate complexity compared to higher-order Trotter-Suzuki formulas such as the Ruth decomposition. In particular, our ansatz with four alternating exponentials outperformed the seven-exponential sequence of the Ruth formula. This highlights the strength of the renormalized global variational principles, which can be tailored to mimic realistic error environments when running simulations on quantum hardware. By explicitly accounting for coherence times, one can design ansätze that are better suited to the hardware constraints. An alternative perspective is to start from a custom-designed quantum circuit composed of a sequence of quantum gates, where the gate rotation angles serve as variational parameters. These parameters can then be optimized on a classical computer using our variational principle and subsequently deployed in quantum simulations on actual devices.

In addition, we briefly discuss several approximate variational techniques, including approximate analytical expressions for the variational parameters which provides renormalized product formulas that give improvements over the equivalent TS decomposition, and a partial-trace method inspired by the Krylov subspace approach. These methods are especially useful in settings where a fully exact treatment is either computationally infeasible or unnecessary.

Our approach offers several notable advantages.

First, it provides a stroboscopic approximation of U(t) that remains accurate over longer time intervals than the Trotter-Suzuki method, which is primarily reliable only at very short times. Unlike state-specific variational techniques, the resulting unitary is state-independent and therefore applicable to any initial state, making it a versatile tool for general-purpose quantum simulation. In addition, the ansatz typically achieves reduced circuit depth while delivering higher accuracy than Trotter-Suzuki formulas of comparable size—a key advantage in the NISQ era. We showed that for some Hamiltonians, our variational approach will provide accuracy superior to higher order TS decompositions. Beyond simulating dynamics, the framework also extends naturally to tasks such as constructing custom, hardware-efficient quantum gates [49, 50]. This is particularly valuable since high-fidelity twoqubit gates remain a major bottleneck in current quantum devices [51, 52]. By enabling the design of specialized circuit ansätze that minimize two-qubit interactions while preserving accuracy, our method directly addresses one of the central challenges in practical quantum computing.

We believe that our findings open promising avenues for real-world applications in quantum computing, with the potential to play a significant role in error mitigation—a cornerstone for advancing the accuracy and practicality of current quantum simulations.

VII. ACKNOWLEDGMENTS

IA and JPFL acknowledges the support of the Natural Sciences and Engineering Research Council of Canada (NSERC) RGPIN-2022-03882 and (NRC) AQC-200-1. MK acknowledges the support from the Applied Quantum Computing Challenge Program at the National Research Council of Canada.

Appendix A: Equations of motion for variational parameters

In this section, we will use Eq. (3) to derive the explicit equations of motion for the three and four exponential ansatz.

1. 3-exponential ansatz

Consider the following time-evolution ansatz that approximates the exact time evolution of a model Hamiltonian ${\cal H}$

$$U_a(t) = e^{ic_0(t)A}e^{ic_1(t)B}e^{ic_2(t)C},$$
(A1)

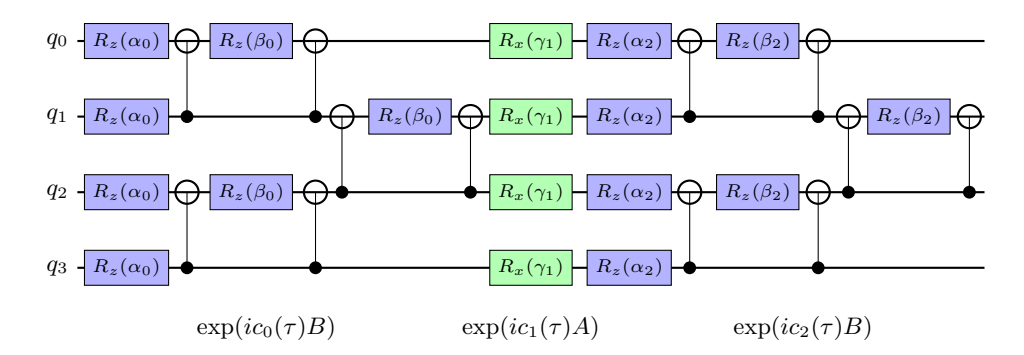


FIG. 11: Quantum circuit implementation of the time-evolution operator $U_a(\tau) = e^{ic_0(\tau)B}e^{ic_1(\tau)A}e^{ic_2(\tau)B}$ for the quantum Ising model [Eq. (28)] with N=4 qubits. Single-qubit rotations R_x implement the transverse field, while longitudinal fields correspond to R_z gates. The two-body ZZ interactions are decomposed into CNOT- R_z -CNOT sequences. The gate angles are given by $\alpha_i = -2c_i(\tau)h_z$, $\beta_i = -2c_i(\tau)J$, and $\gamma_1 = -2c_1(\tau)h_x$.

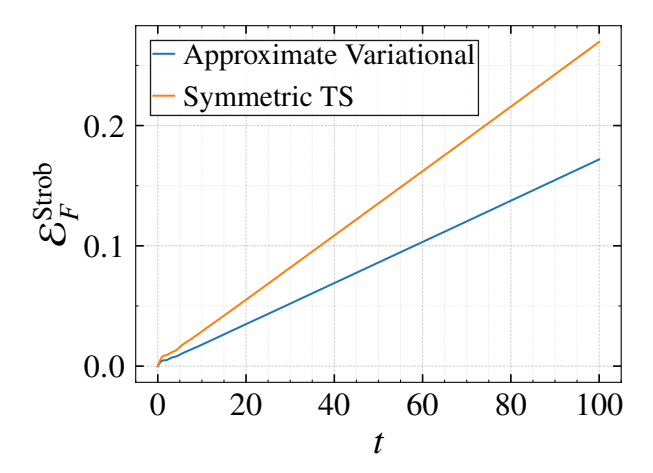


FIG. 12: Stroboscopic error in the time evolution operator of the QIM[Eq.(28)] when comparing the symmetric Trotter–Suzuki decomposition [Eq. (8)] with the approximate variational approach [Eq. (55)]. We set $h_x = h_z = J = 1.0$, N = 5, and time step $\tau = 0.1$. The variational scheme exhibits a consistently smaller error growth with time.

where A, B, and C are Hermitian operators built from terms in H. The ansatz in Eq. (9) is a special case with A = C. The equations of motion for the variational parameters are

$$g_{00}\dot{c_0} + g_{01}\dot{c_1} + g_{02}\dot{c_2} = D_0 \tag{A2}$$

$$g_{10}\dot{c_0} + g_{11}\dot{c_1} + g_{12}\dot{c_2} = D_1 \tag{A3}$$

$$g_{20}\dot{c_0} + g_{21}\dot{c_1} + g_{22}\dot{c_2} = D_2 \tag{A4}$$

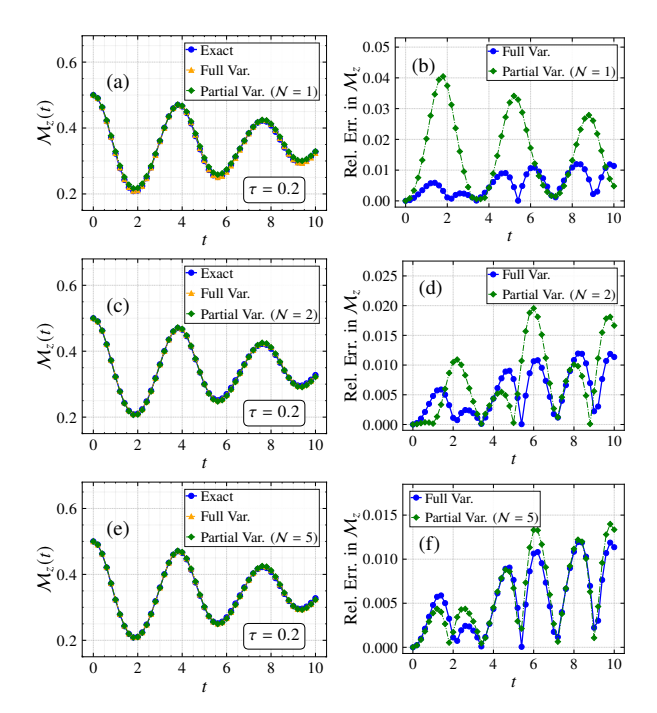


FIG. 13: The stroboscopic magnetization of the quantum Ising model [Eq. (28)] obtained via full and partial traces variational settings with $h_x = h_z = J = 1.0$ and N = 5, using (a) one $(\mathcal{N} = 1)$, (c) two $(\mathcal{N} = 2)$, and (e) five $(\mathcal{N} = 5)$ Krylov basis vectors. (b,d,f) The corresponding relative errors in the dynamical magnetization.

where the quantum metric components g_{ij} read

$$g_{00} = \text{Tr} \left[A^2 \right],$$

$$g_{01} = g_{10} = \text{Tr} \left[AB \right],$$

$$g_{02} = g_{20} = \text{Tr} \left[Ae^{ic_1(t)B}Ce^{-ic_1(t)B} \right],$$

$$g_{11} = \text{Tr} \left[B^2 \right],$$

$$g_{12} = g_{21} = \text{Tr} \left[BC \right],$$

$$g_{22} = \text{Tr} \left[C^2 \right]$$
(A5)

and,

$$D_{0} = -\text{Tr} [AH],$$

$$D_{1} = -\text{Tr} [e^{ic_{0}A}Be^{-ic_{0}A}H],$$

$$D_{2} = -\text{Tr} [e^{ic_{0}A}e^{ic_{1}B}Ce^{-ic_{1}B}e^{-ic_{0}A}H]$$
(A6)

2. 4-exponential ansatz

We further consider the following unitary ansatz

$$U_a(t) = e^{ic_0(t)A} e^{ic_1(t)B} e^{ic_2(t)C} e^{ic_3(t)D},$$
(A7)

where A, B, C, and D are Hermitian operators. Our four exponentials ansatz Eq. (10) is a special case with A = C and B = D.

Computing the entries g_{jk} for (A7) ansatz:

$$g_{00} = \text{Tr} \left[A^2 \right],$$

$$g_{01} = g_{10} = \text{Tr} \left[AB \right],$$

$$g_{02} = g_{20} = \text{Tr} \left[Ae^{ic_1(t)B}Ce^{-ic_1(t)B} \right],$$

$$g_{03} = g_{30} = \text{Tr} \left[Ae^{ic_1(t)B}e^{ic_2(t)C}De^{-ic_2(t)C}e^{-ic_1(t)B} \right],$$

$$g_{11} = \text{Tr} \left[B^2 \right],$$

$$g_{12} = g_{21} = \text{Tr} \left[BC \right],$$

$$g_{13} = g_{31} = \text{Tr} \left[Be^{ic_2(t)C}De^{-ic_2(t)C} \right],$$

$$g_{22} = \text{Tr} \left[C^2 \right],$$

$$g_{23} = g_{32} = \text{Tr} \left[CD \right],$$

$$g_{33} = \text{Tr} \left[D^2 \right].$$
(A8)

and

$$D_{0} = -\text{Tr} [AH],$$

$$D_{1} = -\text{Tr} \left[e^{ic_{0}(t)A} B e^{-ic_{0}(t)A} H \right],$$

$$D_{2} = -\text{Tr} \left[e^{ic_{0}(t)A} e^{ic_{1}(t)B} C e^{-ic_{1}(t)B} e^{-ic_{0}(t)A} H \right],$$

$$D_{3} = -\text{Tr} \left[e^{ic_{0}(t)A} e^{ic_{1}(t)B} e^{ic_{2}(t)C} D e^{-ic_{2}(t)C} e^{-ic_{1}(t)B} e^{-ic_{0}(t)A} H \right].$$
(A9)

Appendix B: Alternative action principles

In this section, we will illustrate few examples of Lagrangians that can be used as basis for our variational principle. The first example we would like to consider is the following Lagrangian [22]

$$\mathcal{L}_2 = ||i\partial_t U - HU||_F^2 \tag{B1}$$

where $||X||_F = \sqrt{\text{Tr}[XX^{\dagger}]}$ is the Frobenius norm of X. One readily finds $\partial_t^2 U + H^2 U = 0$ as variational equations of motion. Of course this is the time derivative of equation (1) and therefore yields identical results if we choose $\dot{U}(0) = -iHU(0)$ as extra initial condition. The later constraint is very important as the second order differential equation have a general solution $U(t) = e^{-iHt}U_1 + e^{iHt}U_2$ and the constraints forces $U_2 = 0$ and we recover the physical time-evolution.

For a time-evolution ansatz U_a expressed in terms of variational parameters $\{c_i(t)\}\$, we obtain the following equations of motion

$$\sum_{k} g_{jk} \ddot{c}_k + \sum_{\ell k} \Gamma_{j,\ell k} \dot{c}_{\ell} \dot{c}_k + 2i \sum_{k} \mathcal{B}_{jk} \dot{c}_k + \mathcal{F}_j = 0$$
(B2)

where g is the quantum metric that appeared earlier in Eq. (3), $\Gamma_{j,\ell k}=\operatorname{Tr}\left[\left(\frac{\partial U_a}{\partial c_j}\right)^\dagger\frac{\partial^2 U_a}{\partial c_\ell\partial c_k}\right]$ is a Christoffel-like symbol derived from the metric g which is classically analogous to the gradient of mass tensor in case of coupled Harmonic oscillators with position dependent effective mass, $\mathcal{B}_{jk}=\operatorname{Tr}\left[\left(\frac{\partial U_a}{\partial c_j}\right)^\dagger H \frac{\partial U_a}{\partial c_k}\right]$ measures how the expectation value of the Hamiltonian (up to a constant) varies with respect to parameters changes throughout the entire Hilbert space which is classically similar to the pseudo-magnetic field that represents variations in the vector potential, and $\mathcal{F}_j=-\operatorname{Tr}\left[\left(\frac{\partial U_a}{\partial c_j}\right)^\dagger H^2 U_a\right]$ is a generalized force derived from a potential $V(c,c^*)=-\operatorname{Tr}\left[U_a^\dagger H^2 U_a\right]$, i.e. $\mathcal{F}_j=\partial_{c^*}V(c,c^*)$.

Although these equations of motion have richer structure compared to the first order differential equations associated with the first variational principle, they have the disadvantage of being second-order non-linear differential equations that are computationally more expensive but still feasible.

In addition, one can also try the following Lagrangian

$$\mathcal{L}_3 = \frac{1}{2} \text{Tr} \left[\dot{U}^{\dagger} \dot{U} - U^{\dagger} H^2 U \right]$$
 (B3)

where the first term is similar to the kinetic energy term for a system of harmonic oscillator and the second term is the just the coupling potential energy with H^2 plays a rule of generalized spring constant matrix. In this case, the equations of motion are

$$\sum_{k} g_{jk} \ddot{c}_k + \sum_{\ell k} \Gamma_{j,\ell k} \dot{c}_{\ell} \dot{c}_k - \mathcal{F}_j = 0$$
(B4)

which are identical to the earlier Lagrangian but this time without the linear *velocity* term. One can even use more constrained Lagrangian

$$\mathcal{L}_4 = \text{Tr}\left[\Lambda^{\dagger} X + X^{\dagger} \Lambda\right] \tag{B5}$$

where $X = i\dot{U} - HU$ is the residual operator. However, we will not exhaust all the possibilities in this work and are left as exercise for the interested reader.

Appendix C: Analytic calculations of the traces

As we discussed in section ??, we derived analytic expressions of the variational parameters for our ansatzs which are expressed in terms of traces of powers of A and B. In this section, we will derive analytic expressions for those traces for the Ising model and the XXZ model with NNN interaction. The idea is based on two facts. First, A spin operator at site j can be expressed as tensor product

$$\sigma_j^{\alpha} = I \otimes I \otimes \dots \otimes \sigma^{\alpha} \otimes I \otimes \dots \otimes I \tag{C1}$$

where $\alpha = x, y, z$ and σ^{α} is the 2 × 2 Pauli matrix. The other identity we will use the following

$$Tr[X \otimes Y] = Tr[X]Tr[Y] \tag{C2}$$

For the transverse field Ising model, we have $A = \frac{J}{4} \sum_{j=1} \sigma_j^z \sigma_{j+1}^z + \frac{h_z}{2} \sum_{j=1}^N \sigma_j^z$ and $B = \frac{h_x}{2} \sum_{j=1}^N \sigma_j^x$. First, one can easily see that Tr[AB] = 0. Next, let's look at the expressions of A^2 and B^2

$$A^{2} = \frac{J^{2}}{16} \sum_{j,m=1}^{N-1} \sigma_{j}^{z} \sigma_{j+1}^{z} \sigma_{m}^{z} \sigma_{m+1}^{z} + \frac{Jh_{z}}{4} \sum_{j=1}^{N-1} \sum_{n=1}^{N} \sigma_{j}^{z} \sigma_{j+1}^{z} \sigma_{n}^{z} + \frac{h_{z}^{2}}{4} \sum_{\ell,n=1}^{N} \sigma_{\ell}^{z} \sigma_{n}^{z}$$
 (C3)

$$B^{2} = \frac{h_{x}^{2}}{4} \sum_{\ell=1}^{N} \sigma_{\ell}^{x} \sigma_{n}^{x} \tag{C4}$$

One can easily verify that $\text{Tr}[B^2] = \frac{N2^N h_x^2}{4}$. Now, for A^2 , let's walk through term by term. For the first term, we expect that non-zero contributions to the trace to come from the case when j=m, giving a total contribution of $\frac{(N-1)2^N J^2}{16}$. Furthermore, the second term in A^2 gives zero contribution to the trace. Finally, the last term contributes $\frac{N2^N h_z^2}{4}$ to the trace. This gives

$$Tr[A^2] = \frac{(N-1)2^N J^2}{16} + \frac{N2^N h_z^2}{4}$$
 (C5)

Now, there are two more traces to compute. First, let's look at A^2B^2

$$A^{2}B^{2} = \frac{Nh_{x}^{2}}{4}A^{2} + \frac{1}{2}h_{x}^{2}A^{2}\sum_{i < j}\sigma_{i}^{x}\sigma_{j}^{x}$$
(C6)

which gives $\text{Tr}[A^2B^2] = \frac{N2^Nh_x^2}{4}\left[(N-1)\frac{J^2}{16} + \frac{Nh_z^2}{4}\right]$. Finally, we also find

$$Tr[(AB)^{2}] = \frac{2^{N}h_{x}^{2}}{4} \left[\frac{J^{2}}{16}(N-1)(N-4) + \frac{h_{z}^{2}}{4}N(N-2) \right]$$
 (C7)

Next, we consider the XXZ model without NNN interaction, we have

$$A = \frac{J_1}{4} \sum_{j:\text{even}}^{N-1} \left[\sigma_j^x \sigma_{j+1}^x + \sigma_j^y \sigma_{j+1}^y + \Delta_1 \sigma_j^z \sigma_{j+1}^z \right]$$
 (C8)

and

$$B = \frac{J_1}{4} \sum_{j:\text{odd}}^{N-1} \left[\sigma_j^x \sigma_{j+1}^x + \sigma_j^y \sigma_{j+1}^y + \Delta_1 \sigma_j^z \sigma_{j+1}^z \right]$$
 (C9)

We find the following traces

$$Tr[A^2] = \frac{J_1^2 2^N (2 + \Delta_1^2)}{16} \sum_{j:\text{even}}^{N-1} = \frac{J_1^2 2^N (2 + \Delta_1^2)}{16} \left\lfloor \frac{N-1}{2} \right\rfloor$$
 (C10)

$$Tr[B^2] = \frac{J_1^2 2^N (2 + \Delta_1^2)}{16} \sum_{j:\text{odd}}^{N-1} = \frac{J_1^2 2^N (2 + \Delta_1^2)}{16} \left\lceil \frac{N-1}{2} \right\rceil$$
 (C11)

$$Tr[A^{2}B^{2}] = \left(\frac{J_{1}}{4}\right)^{4} (2 + \Delta_{1}^{2})^{2} 2^{N} \left\lfloor \frac{N-1}{2} \right\rfloor \left\lceil \frac{N-1}{2} \right\rceil$$
 (C12)

$$Tr[(AB)^{2}] = \left(\frac{J_{1}}{4}\right)^{4} (2 + \Delta_{1}^{2})^{2} 2^{N} \left\lfloor \frac{N-1}{2} \right\rfloor \left\lceil \frac{N-1}{2} \right\rceil - 4 \left(\frac{J_{1}}{4}\right)^{4} (1 + 2\Delta_{1}^{2}) 2^{N} (N-2)$$
 (C13)

and Tr[AB] = 0. Finally, we would like to include the NNN interaction and compute the relevant traces based on the three blocks A, B, and C defined in Eqs. (36)-(38). We list below all the traces appearing in our approximate analytical forms of the variational parameters

$$Tr[A^{2}] = Tr[B^{2}] = \frac{2^{N}}{16} \left[J_{1}^{2}(N-1) + J_{2}^{2}(N-2) \right]$$
 (C14)

$$Tr[C^2] = \frac{2^N}{16} \left[J_1^2 \Delta_1^2 (N-1) + J_2 \Delta_2^2 (N-2) \right]$$
 (C15)

$$Tr[AB] = Tr[AC] = Tr[BC] = 0$$
(C16)

$$Tr[A^2B^2] = 2^{N-8} \left[J_1^2(N-1) + J_2^2(N-2) \right]^2$$
(C17)

$$\operatorname{Tr}[A^2C^2] = \operatorname{Tr}[B^2C^2] = 2^{N-8} \left[\Delta_1^2 J_1^2(N-1) + \Delta_2^2 J_2^2(N-2) \right] \left[J_1^2(N-1) + J_2^2(N-2) \right] \tag{C18}$$

$$Tr[A^{2}BC] = Tr[A^{2}CB] = -\left(\frac{J_{1}}{4}\right)^{2} \frac{J_{2}}{4} \left[\frac{\Delta_{2}J_{2}}{2} + \Delta_{1}J_{1}\right] 2^{N}(N-2)$$
 (C19)

$$\operatorname{Tr}[(AB)^2] = 2^{N-8} \left[J_1^4 (N-3)^2 + 2J_1^2 J_2^2 (N^2 - 11N + 22) + J_2^4 \begin{cases} 1, & \text{if } N = 3, \\ N^2 - 8N + 20, & \text{if } N > 3. \end{cases} \right]$$
(C20)

$$\operatorname{Tr}[(AC)^2] = 2^{N-8} \left[\Delta_1^2 J_1^4 (N-3)^2 + (\Delta_1^2 + \Delta_2^2) J_1^2 J_2^2 (N^2 - 11N + 22) + \Delta_2^2 J_2^4 \begin{cases} 1, & \text{if } N = 3, \\ N^2 - 8N + 20, & \text{if } N > 3. \end{cases} \right]$$
(C21)

$$Tr[(BC)^2] = Tr[(AC)^2]$$
(C22)

and

$$Tr[ABAC] = 2^{N-7}(N-2)J_1^2J_2[2\Delta_1J_1 + \Delta_2J_2]$$
(C23)

- [1] H. Q. Lin. Exact diagonalization of quantum-spin models. *Phys. Rev. B*, 42:6561–6567, Oct 1990.
- [2] J M Zhang and R X Dong. Exact diagonalization: the bose–hubbard model as an example. *European Journal of Physics*, 31(3):591, apr 2010.
- [3] Alexander Wietek and Andreas M. Läuchli. Sublattice coding algorithm and distributed memory parallelization for large-scale exact diagonalizations of quantum many-body systems. *Phys. Rev. E*, 98:033309, Sep 2018.
- [4] Richard P Feynman. Simulating physics with computers. *International Journal of Theoretical* Physics, 21(6-7):467–488, 1982.
- [5] Seth Lloyd. Universal quantum simulators. Science, 273(5278):1073–1078, 1996.
- [6] Dominic W. Berry, Graeme Ahokas, Richard Cleve, and Barry C. Sanders. Efficient quantum algorithms for simulating sparse hamiltonians. Communications in Mathematical Physics, 270(2):359–371, 2007
- [7] William Kirby, Mario Motta, and Antonio Mezzacapo. Exact and efficient lanczos method on a quantum computer. *Quantum*, 7(1018):1018, May 2023.
- [8] Marek Gluza. Double-bracket quantum algorithms for diagonalization. *Quantum*, 8(1316):1316, April 2024.
- [9] Yuya O Nakagawa, Masahiko Kamoshita, Wataru Mizukami, Shotaro Sudo, and Yu-Ya Ohnishi. ADAPT-QSCI: Adaptive construction of an input state for quantum-selected configuration interaction. J. Chem. Theory Comput., 20(24):10817– 10825, December 2024.
- [10] Ryan LaRose, Arkin Tikku, Étude O'Neel-Judy, Lukasz Cincio, and Patrick J Coles. Variational quantum state diagonalization. Npj Quantum Inf.,

- 5(1), June 2019.
- [11] Hale F Trotter. On the product of semi-groups of operators. *Proceedings of the American Mathematical Society*, 10(4):545–551, 1959.
- [12] Masuo Suzuki. General theory of fractal path integrals with applications to many-body theories and statistical physics. *Journal of Mathematical Physics*, 32(2):400–407, 1991.
- [13] John Preskill. Quantum Computing in the NISQ era and beyond. *Quantum*, 2:79, August 2018.
- [14] Kishor Bharti, Alba Cervera-Lierta, Thi Ha Kyaw, Tobias Haug, Sumner Alperin-Lea, Abhinav Anand, Matthias Degroote, Hermanni Heimonen, Jakob S. Kottmann, Tim Menke, Wai-Keong Mok, Sukin Sim, Leong-Chuan Kwek, and Alán Aspuru-Guzik. Noisy intermediate-scale quantum algorithms. Rev. Mod. Phys., 94:015004, Feb 2022.
- [15] Jarrod R McClean, Jonathan Romero, Ryan Babbush, and Alán Aspuru-Guzik. The theory of variational hybrid quantum-classical algorithms. New Journal of Physics, 18(2):023023, feb 2016.
- [16] Yordan S Yordanov, V Armaos, Crispin H W Barnes, and David R M Arvidsson-Shukur. Qubit-excitation-based adaptive variational quantum eigensolver. Commun. Phys., 4(1), October 2021.
- [17] Ho Lun Tang, Yanzhu Chen, Prakriti Biswas, Alicia B. Magann, Christian Arenz, and Sophia E. Economou. Nonvariational adapt algorithm for quantum simulations. *Phys. Rev. Res.*, 7:023275, Jun 2025.
- [18] J Wayne Mullinax, Panagiotis G Anastasiou, Jeffrey Larson, Sophia E Economou, and Norm M Tubman. Classical preoptimization approach for ADAPT-VQE: Maximizing the potential of high-

- performance computing resources to improve quantum simulation of chemical applications. *J. Chem. Theory Comput.*, 21(8):4006–4015, April 2025.
- [19] Xiao Yuan, Suguru Endo, Qi Zhao, Ying Li, and Simon C. Benjamin. Theory of variational quantum simulation. *Quantum*, 3:191, October 2019.
- [20] M Cerezo, Andrew Arrasmith, Ryan Babbush, Simon C Benjamin, Suguru Endo, Keisuke Fujii, Jarrod R McClean, Kosuke Mitarai, Xiao Yuan, Lukasz Cincio, and Patrick J Coles. Variational quantum algorithms. *Nat. Rev. Phys.*, 3(9):625–644, August 2021.
- [21] Jarrod R McClean, Sergio Boixo, Vadim N Smelyanskiy, Ryan Babbush, and Hartmut Neven. Barren plateaus in quantum neural network training landscapes. *Nat. Commun.*, 9(1):4812, November 2018.
- [22] Michael Vogl. Variational principle for the time evolution operator, its usefulness in effective theories of condensed matter systems, and insight into the role played by the quantum geometry of unitary transformations. Eur. Phys. J. Plus, 140(9), September 2025
- [23] H. F. Trotter. On the product of semi-groups of operators. Proceedings of the American Mathematical Society, 10(4):545–551, 1959.
- [24] Masuo Suzuki. Generalized trotter's formula and systematic approximants of exponential operators and inner derivations with applications to manybody problems. *Commun. Math. Phys.*, 51(2):183– 190, June 1976.
- [25] Xiao Yuan, Suguru Endo, Qi Zhao, Ying Li, and Simon C Benjamin. Theory of variational quantum simulation. *Quantum*, 3(191):191, October 2019.
- [26] James Stokes, Josh Izaac, Nathan Killoran, and Giuseppe Carleo. Quantum natural gradient. Quantum, 4(269):269, May 2020.
- [27] Brian C Hall. Lie groups, lie algebras, and representations. In *Graduate Texts in Mathematics*, Graduate texts in mathematics, pages 333–366. Springer New York, New York, NY, 2013.
- [28] J P Serre. Lie algebras and Lie groups: 1964 lectures given at Harvard University. Springer, 2009.
- [29] A A Kirillov. An introduction to Lie groups and Lie algebras, volume 113. Cambridge University Press,
- [30] Yong-Xin Yao, Niladri Gomes, Feng Zhang, Cai-Zhuang Wang, Kai-Ming Ho, Thomas Iadecola, and Peter P. Orth. Adaptive variational quantum dynamics simulations. PRX Quantum, 2:030307, Jul 2021.
- [31] B P Lanyon, C Hempel, D Nigg, M Müller, R Gerritsma, F Zähringer, P Schindler, J T Barreiro, M Rambach, G Kirchmair, M Hennrich, P Zoller, R Blatt, and C F Roos. Universal digital quantum simulation with trapped ions. *Science*, 334(6052):57–61, October 2011.
- [32] Xinhua Peng, Jiangfeng Du, and Dieter Suter. Quantum phase transition of ground-state entanglement in a heisenberg spin chain simulated in an nmr quantum computer. *Phys. Rev. A*, 71:012307, Jan 2005.

- [33] R Barends, A Shabani, L Lamata, J Kelly, A Mezzacapo, U Las Heras, R Babbush, A G Fowler, B Campbell, Yu Chen, Z Chen, B Chiaro, A Dunsworth, E Jeffrey, E Lucero, A Megrant, J Y Mutus, M Neeley, C Neill, P J J O'Malley, C Quintana, P Roushan, D Sank, A Vainsencher, J Wenner, T C White, E Solano, H Neven, and John M Martinis. Digitized adiabatic quantum computing with a superconducting circuit. Nature, 534(7606):222–226, June 2016.
- [34] P Pfeuty. The one-dimensional ising model with a transverse field. ANNALS of Physics, 57(1):79–90, 1970
- [35] Subir Sachdev. Quantum phase transitions. Phys. World, 12(4):33–38, April 1999.
- [36] T. K. Kopeć, K. D. Usadel, and G. Büttner. Instabilities in the quantum sherrington-kirkpatrick ising spin glass in transverse and longitudinal fields. *Phys. Rev. B*, 39:12418–12421, Jun 1989.
- [37] Ronald D. Ruth. A canonical integration technique. IEEE Transactions on Nuclear Science, 30(4):2669– 2671, 1983.
- [38] Etienne Forest and Ronald D. Ruth. Fourth-order symplectic integration. *Physica D: Nonlinear Phe*nomena, 43(1):105–117, 1990.
- [39] Sangjin Lee, Youngseok Kim, and Seung-Woo Lee. Trotter error mitigation by error profiling with shallow quantum circuit, 2025.
- [40] Michio Jimbo, Kei Miki, Tetsuji Miwa, and Atsushi Nakayashiki. Correlation functions of the xxz model for Δ ; -1. Physics Letters A, 168(4):256–263, 1992.
- [41] Mohammad F. Maghrebi, Zhe-Xuan Gong, and Alexey V. Gorshkov. Continuous symmetry breaking in 1d long-range interacting quantum systems. *Phys. Rev. Lett.*, 119:023001, Jul 2017.
- [42] Shi-Jian Gu, Hai-Qing Lin, and You-Quan Li. Entanglement, quantum phase transition, and scaling in the XXZ chain. *Phys. Rev. A*, 68:042330, Oct 2003.
- [43] Irénée Frérot, Piero Naldesi, and Tommaso Roscilde. Entanglement and fluctuations in the xxz model with power-law interactions. *Phys. Rev. B*, 95:245111, Jun 2017.
- [44] B. N. Narozhny, A. J. Millis, and N. Andrei. Transport in the XXZ model. *Phys. Rev. B*, 58:R2921–R2924, Aug 1998.
- [45] R. D. Somma and A. A. Aligia. Phase diagram of the xxz chain with next-nearest-neighbor interactions. Phys. Rev. B, 64:024410, Jun 2001.
- [46] R. Jafari and A. Langari. Phase diagram of the one-dimensional $s=\frac{1}{2}~xxz$ model with ferromagnetic nearest-neighbor and antiferromagnetic next-nearest-neighbor interactions. *Phys. Rev. B*, 76:014412, Jul 2007.
- [47] C F Van Loan and G Golub. Matrix computations (johns hopkins studies in mathematical sciences). Matrix Computations, 5, 1996.
- [48] B N Parlett. The symmetric eigenvalue problem. Society for Industrial and Applied Mathematics, 1998.
- [49] Eduardo A. Coello Pérez, Joey Bonitati, Dean Lee, Sofia Quaglioni, and Kyle A. Wendt. Quantum

- state preparation by adiabatic evolution with custom gates. Phys. Rev. A, 105:032403, Mar 2022.
- [50] Cristina Cîrstoiu, Zoë Holmes, Joseph Iosue, Lukasz Cincio, Patrick J Coles, and Andrew Sornborger. Variational fast forwarding for quantum simulation beyond the coherence time. Npj Quantum Inf., 6(1), September 2020.
- [51] Frank Arute et al. Quantum supremacy using a programmable superconducting processor. *Nature*, 574(7779):505–510, October 2019.
- [52] P. Krantz, M. Kjaergaard, F. Yan, T. P. Orlando, S. Gustavsson, and W. D. Oliver. A quantum engineer's guide to superconducting qubits. *Applied Physics Reviews*, 6(2):021318, 06 2019.